UILU-ENG 84-3614

Report No. 114

EFFECTS OF OPTICAL EMISSIONS FROM WELD ARCS ON THE PERFORMANCE OF WELDING ROBOT VISION SYSTEMS

by

A. L. Lenef and C. S. Gardner
Department of Electrical Engineering

Supported by
Contract No. US Army CERL
DACA88-83-C-0003
DACA88-84-C-0003

A Report of the

MATERIALS ENGINEERING - MECHANICAL BEHAVIOR

College of Engineering, University of Illinois at Urbana-Champaign

November 1984

ABSTRACT

Many arc welding robots employ one-pass vision systems which use a laser projection and optical triangulation technique for seam tracking. The seam tracking accuracy of these arc welding robots can be adversly affected by the intense optical emissions produced by the weld arc. Optical filtering is generally employed to restrict the spectral bandwidth of these emissions. In this paper, we present absolute intensity measurements of weld arc spectra at visible and near IR wavelengths using $Ar-O_2$ shield gas with solid wire and CO_2 shield gas with flux cored wire. By simulating the effect of an interference filter on the weld arc emissions, these measurements can be used to calculate estimates of the stray arc light visible to a seam tracking camera. These results are useful in determing the optimum wavelength, laser power, and optical filter bandwidth for a particular welding application.

TABLE OF CONTENTS

LIST OF TABLES

LIST OF FIGURES

1. INTRODUCTION

Arc welding robots are making a significant impact in the heavy manufacturing industries. To produce high quality welds, the robots must accurately track the seam formed by the workpieces. Various seam tracking schemes have been proposed and implemented. However, the most recent trend is toward the use of one-pass vision systems which employ a pattern projection and optical triangulation technique to accurately estimate the location of the seam [1-7]. Unlike two-pass tracking systems, these one-pass vision systems can compensate for warpage and changes in alignment which occur during the weld and eliminate the need for elaborate, expensive fixtures to accurately position the workpiece. Vision is very desirable since it can be used to measure the joint topology to provide accurate, non-contact seam tracking of a variety of joints. Vision can also be used to inspect the molten weldpool to provide additional information for adaptive quality control of the welding process. This powerful vision application is used in the arc welding robots developed by Oxford Unversity and General Electric [8], [9].

One of the major difficulties associated with design and use of a welding robot vision system is how to view the projected pattern in the proximity of the intense arc. Projected patterns are often only a few centimeters from the arc. The intensities of the projected patterns are limited by the small, relatively low power illuminating lasers. The background illumination from the arc can be reduced by positioning the camera so that it does not view the arc directly and by using a narrowband interference filter to block most of the reflected, broadband arc radiation.

However, the center wavelength of the interference filter and laser must be carefully chosen to avoid regions of the arc spectrum containing strong line emissions from the plasma constituents. This requirement can be difficult to satisfy if different shield gases are used because their emission spectra vary widely. Furthermore, the center wavelength of the filter depends on temperature and the angle of incident light. Elevated temperatures in the welding environment and changing angles of incidence across the field of view limit filter bandwidths to values greater than about 10 Å. Even the reflected arc radiation from weaker emission lines can be quite intense and reduce the tracking accuracy of the vision system.

In this paper, we present absolute intensity measurements of weld arc spectra at visible and near IR wavelengths using Ar shield gas with solid wire and CO_2 shield gas with flux wire. These measurements include the spectral regions near the He-Ne laser wavelength at 6328 Å and most near IR laser diode wavelengths. By simulating the effect of an interference filter, these measurements can be used to calculate estimates of the intensity of the stray arc light visible to a seam tracking camera. These estimates can be made at different laser wavelengths for common interference filter bandwidths. These results are useful in determining the optimum wavelength, laser power, and interference filter bandwidth for a particular welding application. The estimates are also useful for evaluating the performance of seam tracking algorithoms.

We also present UV and IR weld arc spectra from 3150 - 4250 Å and from 7350 - 9950 Å. These spectra expand a previous catalog of weld arc spectra [10].

2. INTENSITY OF THE BACKGROUND ARC ILLUMINATION

2.1 The Vision System

Figure 1 is a diagram of a typical welding vision system. It illustrates the triangulation technique used to produce an image of the joint cross section. A laser beam illuminates the workpieces obliquely, making a stripe across the joint. The figure shows the workpiece edges and the gap between the workpieces. When viewed normal to the workpiece, the image appears to have a discontinuity with a length proportional to the height of the gap. When viewed by the camera, the length of the discontinuity is

$$L' = \frac{mH}{\tan \theta} , \qquad (1)$$

where L' = length of discontinuity

H = height of gap

θ = angle of incidence of laser sheet

m = lens magnification.

Figure 2 shows examples of welding robot vision systems from Oxford University and from the National Research Council of Canada (NRCC). Both systems consist of a laser projection unit and a solid state camera which are adjacent to the moving weld torch. The interference filters are located next to the camera lenses. Although laser diodes are utilized for pattern generation in these systems, He-Ne lasers are also commonly used. The Hitachi vision system is an example [1]. Vision systems may also employ special optical arrangements to produce higher intensity stripes than can normally be obtained with a focusing lens. One example is the Advanced

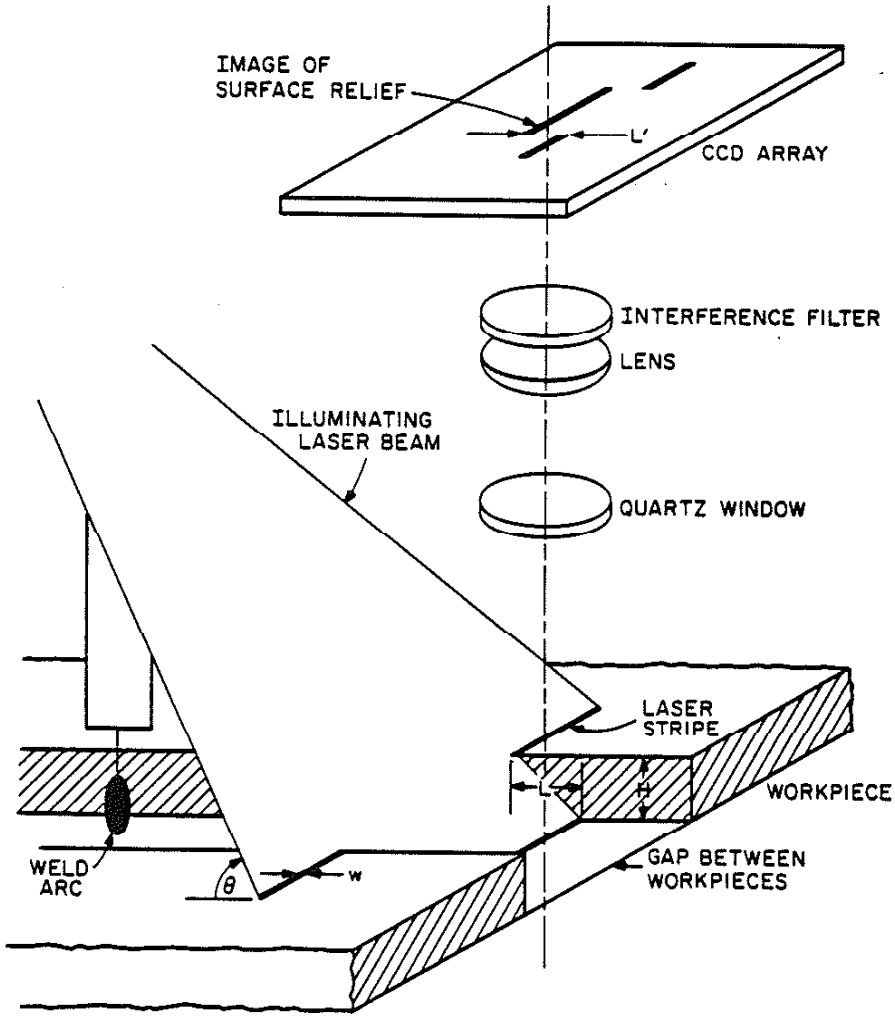

Figure 1. Diagram of typical welding vision system.

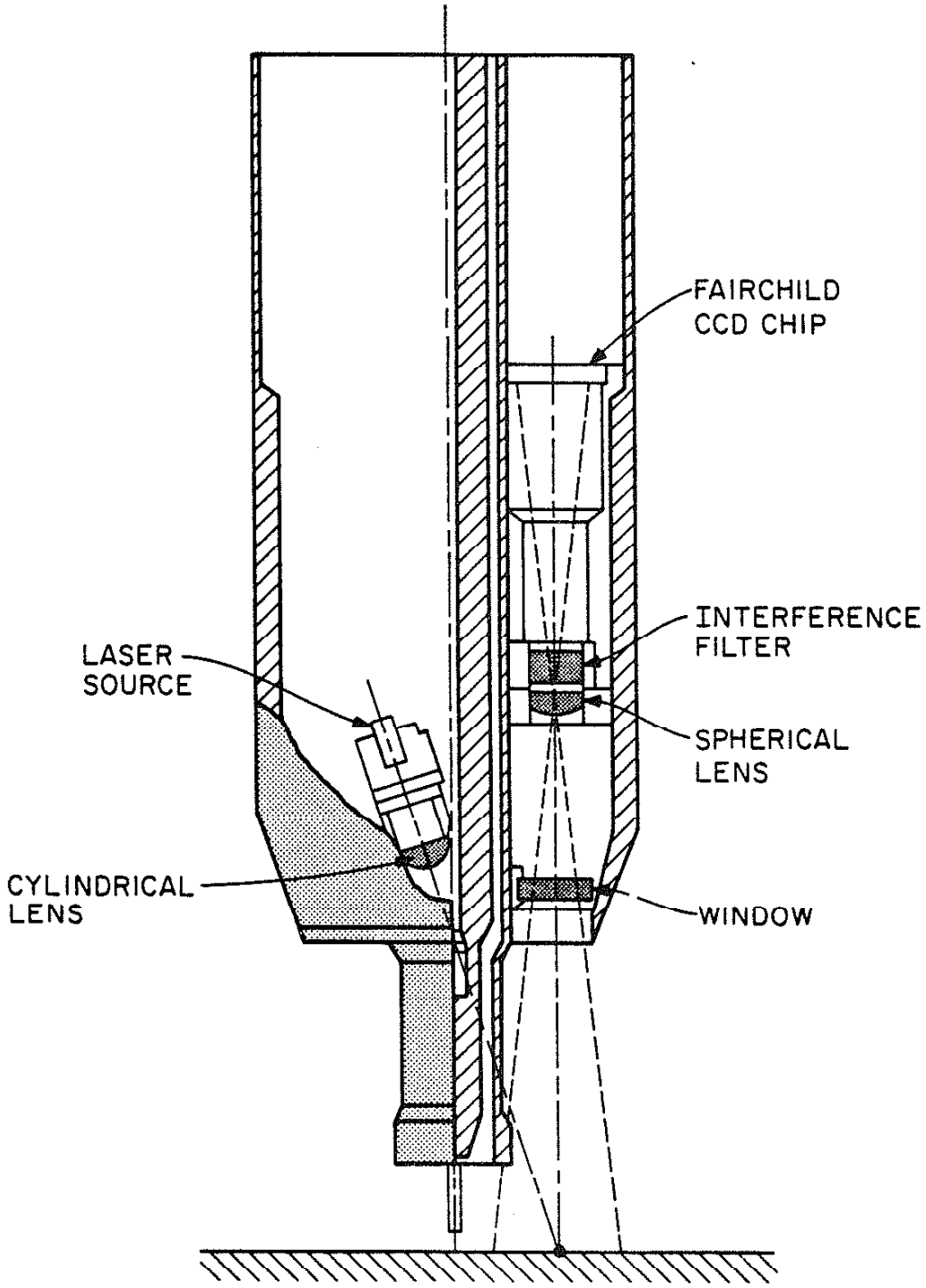

Figure 2a. The Oxford University arc weld vision system. (Adapted from [8].)

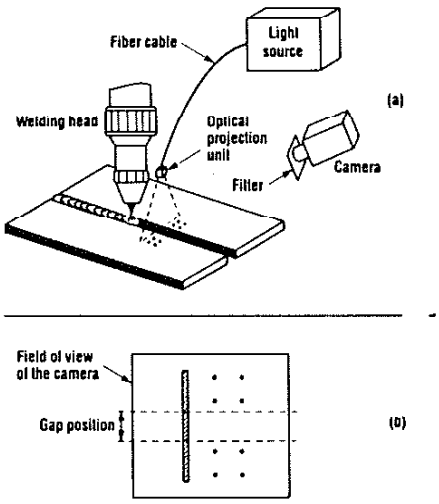

Figure 2b. The NRCC arc weld vision system: (a) overview of the system; (b) typical projected light pattern. (Reprinted from [5].)

Robitics system which employs a rotating mirror arrangement [2].

The background light which illuminates the camera's field of view (FOV) is primarly from workpiece reflections of the extremely bright arc plasma. Other bright sources of light which may contribute to the overall background illumination include brightly lit welding spatters which pass through the FOV (see [1]) and workpiece reflections of molten metal droplets in the arc region. The weldpool, although a bright source of light, is generally not seen by the camera because it is usually outside the FOV and not subject to workpiece reflections. Moreover, it is much cooler than the arc, radiating most of its energy beyond 1.5 μm. The hot, effluent gases near the arc region would not be expected to produce significant amounts of radiation in the visible and near IR because of their very low emissitivity [11].

2.2 Irradiance of the Arc Plasma

To estimate the intensity of the background illumination, the arc plasma will be assumed to be the primary source of light. For reference, a brief summary of the radiometric quantities to be used is included in Table 1.

The arc plasma can be treated as an extended source. The spectral radiant intensity (power per unit solid angle, per unit wavelength) of the arc plasma can be determined from its source area and its average spectral radiance. Referring to Figure 3, the total flux radiated into a solid angle $d\Omega$ from emissions along an optical path which traverses the arc is the radiance at a point (x,y,z) on the arc plasma surface. The optical path is in the direction of the line of sight. The spectral radiance, $L_a(x,y,z,\lambda)$, is the radiance per unit wavelength. $L_a(x,y,z,\lambda)$ depends upon the length of

TABLE 1

SUMMARY OF RADIOMETRIC QUANTITIES

(Adapted from the RCA Electro-Optics Handbook, [12])

QUANTITY	SYMBOL	DESCRIPTION	SI UNITS
Radiant energy	Q		J
Radiant density	w	Energy density	J/m^2
Radiant flux	Φ	Radiated power	J/s
Radiant flux density at a surface:		Power per unit area	W/m^2
Radiant exitance	M	Radiant flux leaving a surface	W/m^2
Irradiance	E	Radiant flux arriving at a surface	W/m^2
Radiant intensity	I	Power radiated by a point source into a solid angle $d\Omega$	W/sr
Radiance	L	Power radiated by a point on an emitting surface into a solid angle $d\Omega$, per unit projected area of the emitting surface	$W/sr \cdot m^2$

Note: The spectral equivalents of the radiometric quantities are per unit wavelength in $\mathring{A}$.

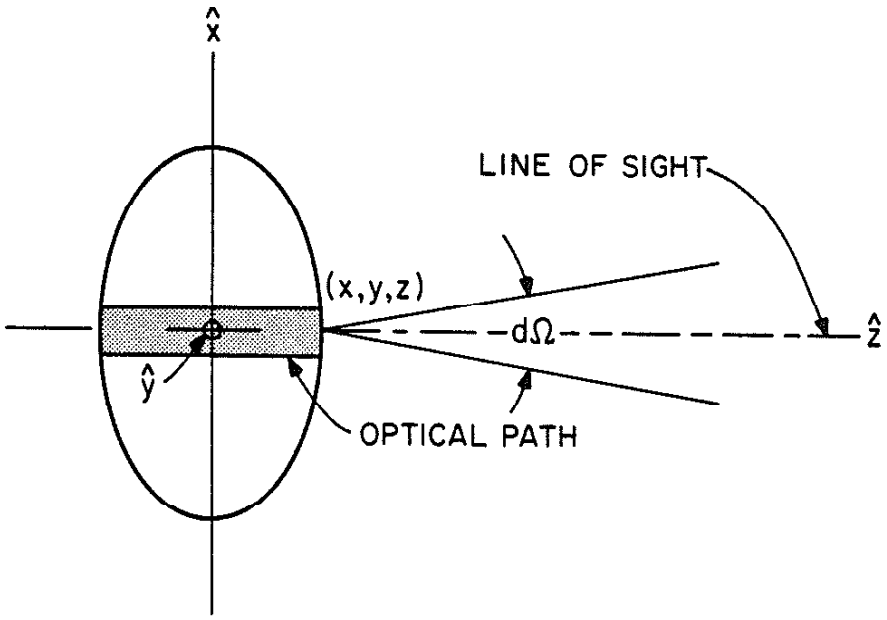

Figure 3. Diagram of an optical path in the weld arc plasma.

the optical path, temperature distribution, and densities of electrons and atoms along the optical path. The spectral radiant intensity of the arc is obtained by integrating across the x-y plane. We have

$$I_a(\lambda) = \int L_a(x,y,z,\lambda)\, dxdy = L_a(\lambda)\, A_s \,, \qquad (2)$$

where $I_a(\lambda)$ = spectral radiant intensity of arc plasma

$L_a(\lambda)$ = average spectral radiance of arc plasma

A_s = source area.

A_s is the projected area of the arc in the direction of the line of sight.

Since the intensity of illumination from the reflected arc is of interest, the reflection properties of the various surfaces encountered in welding also need to be considered. Most surfaces likely to be encountered are optically rough. These surfaces tend to be Lambertian and scatter light uniformly at each point on the surface. A Lambertian surface radiates according to

$$I(\lambda,\theta) = I(\lambda,0) \cos\theta \,, \qquad (3)$$

where θ is the angle of the reflected light from the surface normal. A workpiece that is optically smooth but not mirror-like has slightly different reflection characteristics. The reflected light from a normally incident source is uniformly scattered, while at grazing incidence, the reflection becomes mirror-like. A smooth surface that is free of oxidation is optically smooth. Portions of the workpiece may also produce specular reflections as a result of glints which occur from grinding or cutting of the workpiece.

Figure 4 shows the arrangement of the arc and the workpiece surface.

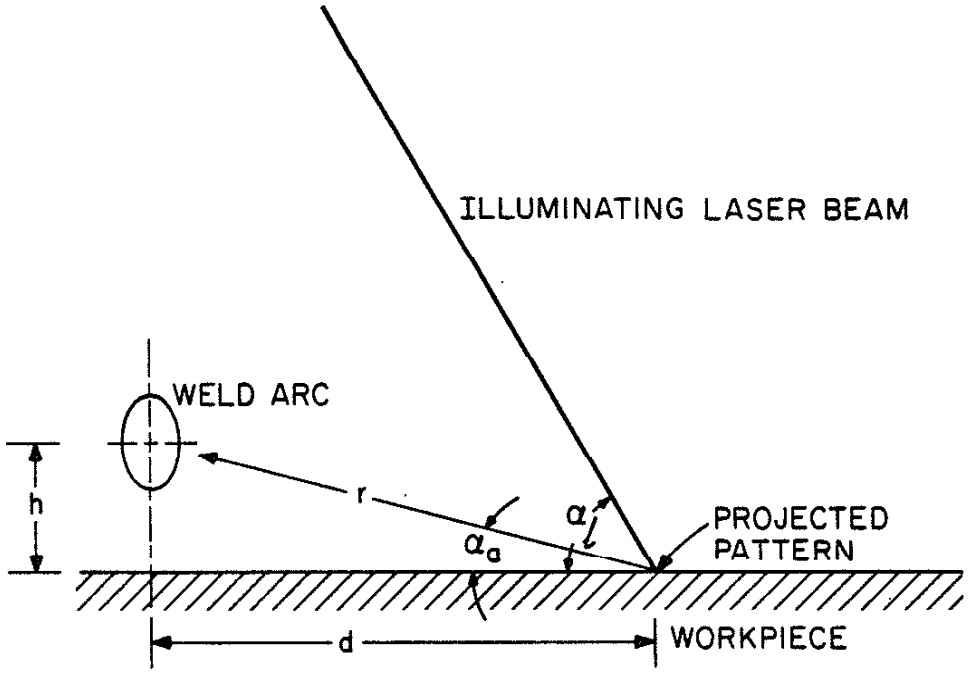

Figure 4. Arrangement of the weld arc and workpiece surface.

The projected pattern is a distance d from the arc axis. The arc is centered about its hottest point which is a distance h above the workpiece; r is the distance from the center of the arc plasma to the projected pattern on the workpiece. We assume that the laser is incident on the workpiece at an angle α_ℓ and illuminates a small area A_p. The solid angle of the incident arc light intercepted by the area A_p is approximately

$$\Omega_p = \frac{A_p}{r^2} \sin \alpha_a \quad , \tag{4}$$

where α_a is the angle of incidence of the arc. We can account for the interference filter used in a vision system by weighting the spectral radiance of the arc with spectral response of the filter. Thus the power of the filtered arc which illuminates the area A_p on the workpiece is given by

$$P_a = \Omega_p \int I_a(\lambda)\, F(\lambda)\, d\lambda = \frac{A_p}{r^2} \sin \alpha_a\, A_s \int L_a(\lambda)\, F(\lambda)\, d\lambda \quad , \tag{5}$$

where $F(\lambda)$ is the filter transmittance and where $A_s L_a(\lambda)$ is the spectral radiant intensity of the arc, $I_a(\lambda)$ (Eq. (2)). The irradiance of the filtered arc on the surface of the workpiece in the vicinity of the pattern is then

$$E_a = \frac{\sin \alpha_a}{r^2} A_s \int L_a(\lambda)\, F(\lambda)\, d\lambda \quad . \tag{6}$$

If the workpiece is assumed to be a Lambertian surface, a simple expression for the signal-to-noise ratio of the camera image plane can be derived. If the laser power is P_ℓ and the laser spot area is A_ℓ, the irradiance of the laser is

$$E_{\ell} = \frac{P_{\ell}}{A_p} = P_{\ell} \frac{\sin \alpha_{\ell}}{A_{\ell}} \quad . \tag{7}$$

Assuming the arc is the primary source of noise, the approximate signal-to-noise ratio at the workpiece is

$$SNR = \frac{E_{\ell}}{E_a} = \frac{\sin \alpha_{\ell}}{\sin \alpha_a} \frac{r^2}{A_{\ell}} \frac{P_{\ell}}{A_s \int L_a(\lambda)\, F(\lambda)\, d\lambda} \quad . \tag{8}$$

Since the surface is diffuse, this is also the SNR at the camera image plane. Equation (8) also gives a lower bound to the actual image sensor SNR if the surface is optically smooth. The reason is that a smooth surface reflects a larger proportion of the incident arc light outside of the lens aperature because the arc is near grazing incidence.

3. SPECTROMETRIC MEASUREMENTS OF ARC PLASMA

The primary experimental objective was to measure the spectral radiance of a weld arc plasma in the regions from 6100 - 6500 Å and from 7600 - 9200 Å for both Ar and CO_2 shielded arcs under typical welding conditions. We could not obtain an accurate measurement of the arc source area although it is probably on the order of 0.5 cm^2. Thus our measurements are in terms of the spectral radiant intensity of the arc. These measurements were made by normalizing the weld arc spectra to power measurements obtained over a small region in the visible red.

3.1 Description of Welding

All welding was performed on a semiautomatic GMA welder with adjustable travel speed. Welding consisted of depositing a single bead on ASTM-242 high strength steel plate. The shield gas mixtures were 98% Ar and 2% O_2 for the first set of measurements and 100% CO_2 for the second set. E70S-3 solid electrode wire was used with the Ar shield gas and E70T-1 flux-cored wire was used with the CO_2 shield gas. The base metal composition is given in Table 2 and the electrode wire compositions are given in Table 3. The nominal electrode height was 2 cm. The travel speed was 25 cm/min. The voltage and current were 30 V and 300 A, respectively.

3.2 Spectral Data Aquisition System

Figure 5 is a block diagram of the system used to measure the weld arc spectra. A 50 mm focal length lens collects the arc light, focusing it onto the end of an armoured, Dolan-Jenner glass fiber bundle. The lens is aimed at the center of the arc and travels with the torch head. A Pyrex cover

TABLE 2

ASTM 242 LOW ALLOY STEEL COMPOSITION (%)

C	0.12
Mn	0.25
P	0.07 - 0.15
S	0.05 max
Si	0.25 - 0.55
Cu	0.25 - 0.40
Cr	0.40 - 0.65
V	0.02 - 0.10
Fe	remainder

TABLE 3

ELECTRODE WIRE COMPOSITIONS

E70S-3 Solid Welding Wire Composition (%)

C	0.06 - 0.15
Mn	0.9 - 1.4
Si	0.45 - 0.70
P	0.025 max
S	0.35 max

E70T-1 Flux Cored Wire Composition (%)

P	0.04
S	0.03
V	0.08
Si	0.9
Ni	0.5
Cr	0.2
Mo	0.3
Mn	1.75
Al	1.8
C	2.0

Flux: Ca, K, Ti, Al, Mg

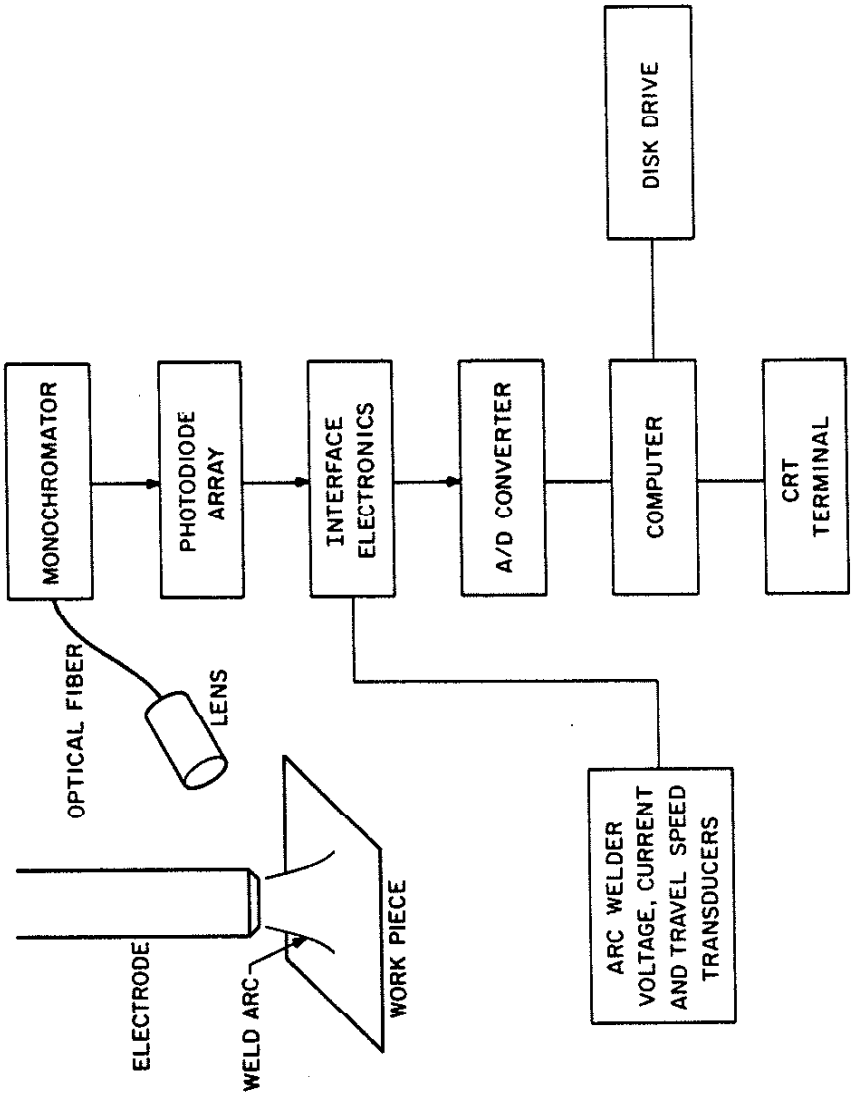

Figure 5. Block diagram of spectral data aquisition system.

protects the lens from welding spatter. The other end of the fiber bundle is placed at the entrance slit of an ISA HR-320 monochromator which uses a 0.32 m focal length Czerny-Turner arrangement [13]. The monochromator is configured as a spectrograph with the exit slit replaced by a 1024 element Reticon array. A 1200 lines/mm holographic grating is used to provide an overall bandwidth of 500 Å. An LSI 11/23 microcomputer is used in conjunction with an ADAC 12 bit A/D converter and direct memory access (DMA) unit for data aquisition and processing of the spectral data. A parallel port and external synchronizing circuit provide the appropriate timing signals for A/D conversion of the Reticon video signal. Spectra are stored on eight inch floppy disks.

The system acquires data in the following manner. The Reticon video circuits continuously scan the array. One entire scan is adjusted to take approximately 50 ms. Each scan consists of a 25 ms array video signal pulse followed by a 25 ms blanking pulse. The slow scan rate allows the charged coupled photodetectors to integrate over a long period of time, making it possible to observe weaker spectra. The video circuits generate three signals: a start pulse which identifies the beginning of each scan, a 0-3 V video signal, and a clock which determines the scan rate. At the desired sampling instant, one of the parallel interface outputs is set to synchronize the A/D converter and DMA with the Reticon start pulse and the Reticon clock. Conversions begin with the initiation of the start pulse. After an array scan is completed, the parallel interface output is reset. Usually, several consecutive array scans are made and summed together before being stored on a floppy disk. This helps reduce noise. The data aquisition sequence can be repeated up to 100 times during a weld run at a

rate of two spectral scans per second. Once saved on floppy, the spectral data sets are averaged and normalized to the Reticon array voltages. Since the Reticon signal contains a small bias voltage, an extra set of scans are taken without welding and later subtracted from the averaged spectral data set.

3.3 Theory and Procedure

To normalize the arc spectra, we must first consider the relatonship between the Reticon array voltages and the spectral radiant intensity of the arc, $A_s L_a(\lambda)$. Since the linearity of the Reticon array is better than ten percent, we will assume that the diode array voltages are proportional to the spectral intensity of the arc. We can write

$$R(\lambda)\, A_s L_a(\lambda) = k V_D(\lambda) \quad , \tag{9}$$

where $R(\lambda)$ = overall spectral response of optics and detector array

k = normalization constant

$V_D(\lambda)$ = diode array voltages.

The overall spectral response $R(\lambda)$ is primarly a function of the fiber optic bundle and detector array since the lens and monochromator have typically uniform spectral responses throughout the visible and near IR spectrum. The normalization constant includes the solid angle of the lens, the array responsivity, and various gain factors. The Pyrex lens cover was not used in these experiments to eliminate uncertainties in the overall spectral response. Figure 6 is a plot of the spectral response of the Dolan-Jenner fiber optic bundle. Figure 7 is a plot of the Reticon array spectral response. From 0.6 - 1.0 μm, the spectral response of the fiber is fairly

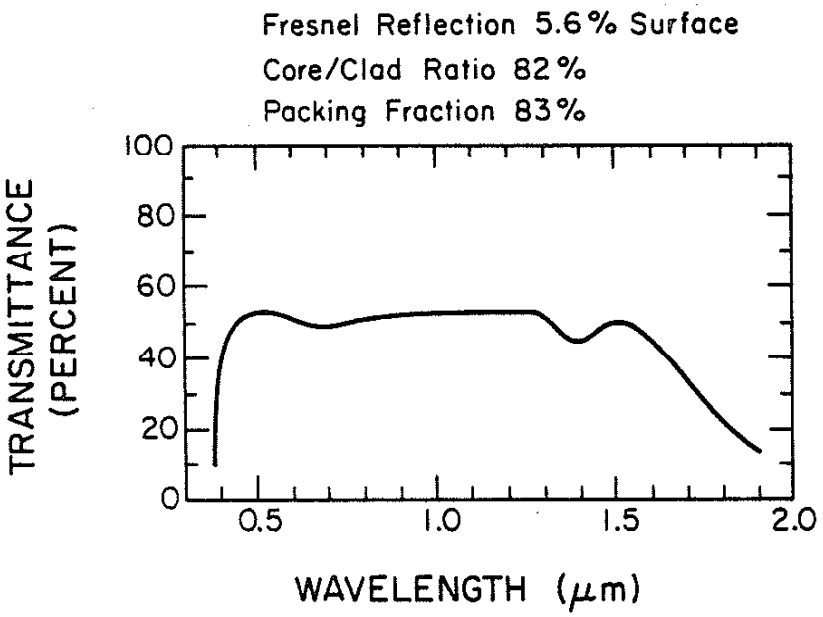

Figure 6. Spectral response of Dolan-Jenner fiber optic bundle.

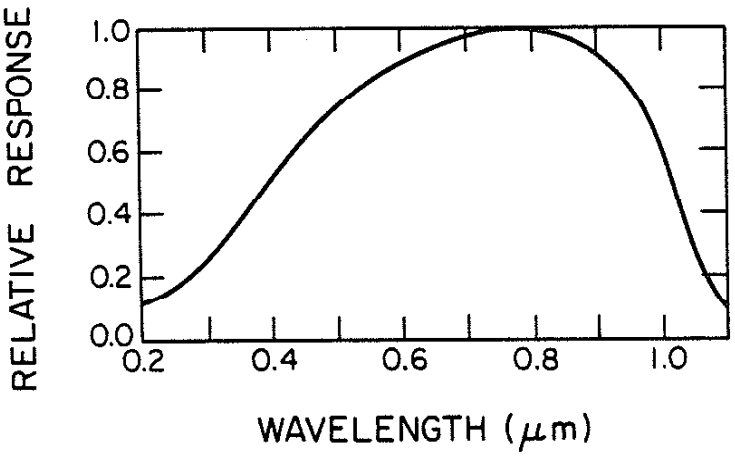

Figure 7. Spectral response of Reticon array.

uniform. However, the Reticon array is nonuniform in this region. We will assume $R(\lambda)$ to be only the spectral response of the array. To evaluate the normalization constant, we measured the arc power with an interference filter placed on the detector of a power meter. The experimental setup is shown in Figure 8. The total power intercepted by the detector is

$$P_M = \Omega_M A_s \int L_a(\lambda) F(\lambda) d\lambda \quad , \tag{10}$$

where P_M = measured power intercepted by photodetector

Ω_M = solid angle intercepted by photodetector

A_s = source area of arc

$L_a(\lambda)$ = spectral radiance of arc

$F(\lambda)$ = spectral response of intereference filter.

The solid angle Ω_M is approximately

$$\Omega_M = \frac{\pi(D/2)^2}{L^2} \quad , \tag{11}$$

where D = diameter of photodetector

L = distance between arc and photodetector.

If a spectral data set is then taken with the identical interference filter placed in front of the lens and then integrated, Equation (9) becomes

$$R(\lambda_c) A_s \int L_a(\lambda) F(\lambda) d\lambda = k \int V_D(\lambda) F(\lambda) d\lambda \quad , \tag{12}$$

where $R(\lambda_c)$ is the array responsivity at the interference filter center wavelength. Combining Equations (10) and (12) to solve for the normalization constant, we have

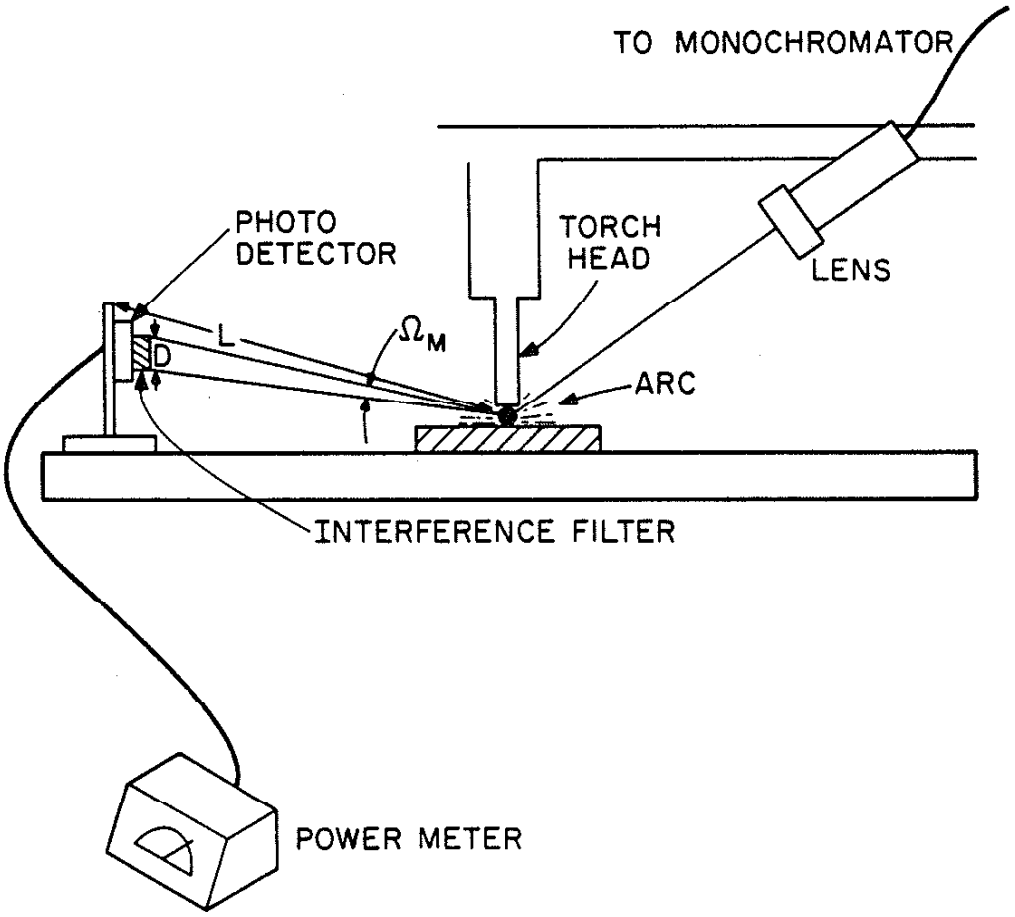

Figure 8. Experimental setup used for the normalization of GMA spectra.

$$k = \frac{R(\lambda_c)\, P_M}{\Omega_M \int V_D(\lambda)\, F(\lambda)\, d\lambda} \quad . \tag{13}$$

Equation (9) then becomes

$$A_s L_a(\lambda) = \frac{R(\lambda_c)}{R(\lambda)} \frac{P_M V_D(\lambda)}{\Omega_M \int V_D(\lambda)\, F(\lambda)\, d\lambda} \quad . \tag{14}$$

Equation (14) is the radiant flux density of the arc in terms of the diode array voltages.

To obtain calibrated spectral data in terms of the arc spectral radiant intensity, we first made several passes with the welder to obtain a consistent power measurement. The arc power was measured using a LICONIX power meter. An interference filter was placed over the photodetector. The power intercepted by the photodetector was taken to be the average of the minimum and maximum readings recorded as the arc passed. The interference filter was then placed over the lens and twenty spectral scans were recorded on a floppy disk with the monochromator center wavelength at 6500 Å. The filter was then removed and five more spectral data sets were recorded, covering the desired spectral regions. Each data set consisted of twenty spectral scans. A set of scans was taken without welding to record the bias voltage and nonrandom noise. Throughout the procedure, the monochromator slit width and orientation of the lens were unaltered. This procedure was performed twice, first using Ar shield gas with solid wire and then using CO_2 shield gas with flux cored wire. Each spectral scan consisted of eight

summed array scans.

Signal processing consisted of averaging each data set with the bias voltage subtracted. The spectra were calibrated using known spectral lines emitted by the arc. A large slit width was used to recover the low amplitude background radiation and the weaker, visible red spectra used for normalizing the arc spectra. Unfortunately, this caused some of the strongest lines to saturate the array elements. To correct for the saturation effect, unsaturated spectra, under identical welding conditions, were taken with a reduced monochromator slit width. A scale factor relating the intensities of the saturated and unsaturated sets was determined from ratios of unsaturated lines. The saturated spectral lines were then replaced by scaled, unsaturated lines.

Details of the power meter measurements and values of the experimental parameters are given in Table 4. Dimensions are those described in Figure 8. The interference filter used was a Melles-Griot hydrogen filter with a center wavelength of 6563 Å and a FWHM of 100 Å. Figure 9 is a plot of its spectral response. Filtered spectra were taken from 6250 - 6750 Å. The interval of integration was only 6450 - 6700 Å to reduce the effects of an imperfectly subtracted bias and quantization error. Although the offset could have been a result of residual transmittance of the interference filter, Figure 9 does not indicate this. The source size of the arc was estimated from photographs and from typical temperature profiles of an arc plasma [14]. Mean estimates of the normalization constants were computed from Equation (13). Variations in the normalization constants can be as great as ±25% because of large fluctuations in the arc intensity.

To aid in choosing the proper interference filter used with the vision

TABLE 4

EXPERIMENTAL PARAMETERS FOR DETERMINATION OF k

QUANTITY	MEASURED VALUES (Ar)	MEASURED VALUES (CO_2)
P_M	0.018 - 0.022 mW	0.010 - 0.016 mW
Avg. P_M	0.020 mW	0.013 mW
L	61.6 cm	56.6 cm
D	0.7 cm	0.7 cm
A_s	0.50 cm^2	0.50 cm^2
Ω_M	1.01×10^{-4} sr	1.21×10^{-4} sr
$R(\lambda_c)$ (λ_c = 6563 Å)	.95	.95
$\int V_D(\lambda)\, F(\lambda)\, d\lambda$	2.93 V·Å	10.1 V·Å
k	0.064 W/sr·Å·V	0.010 W/sr·Å·V

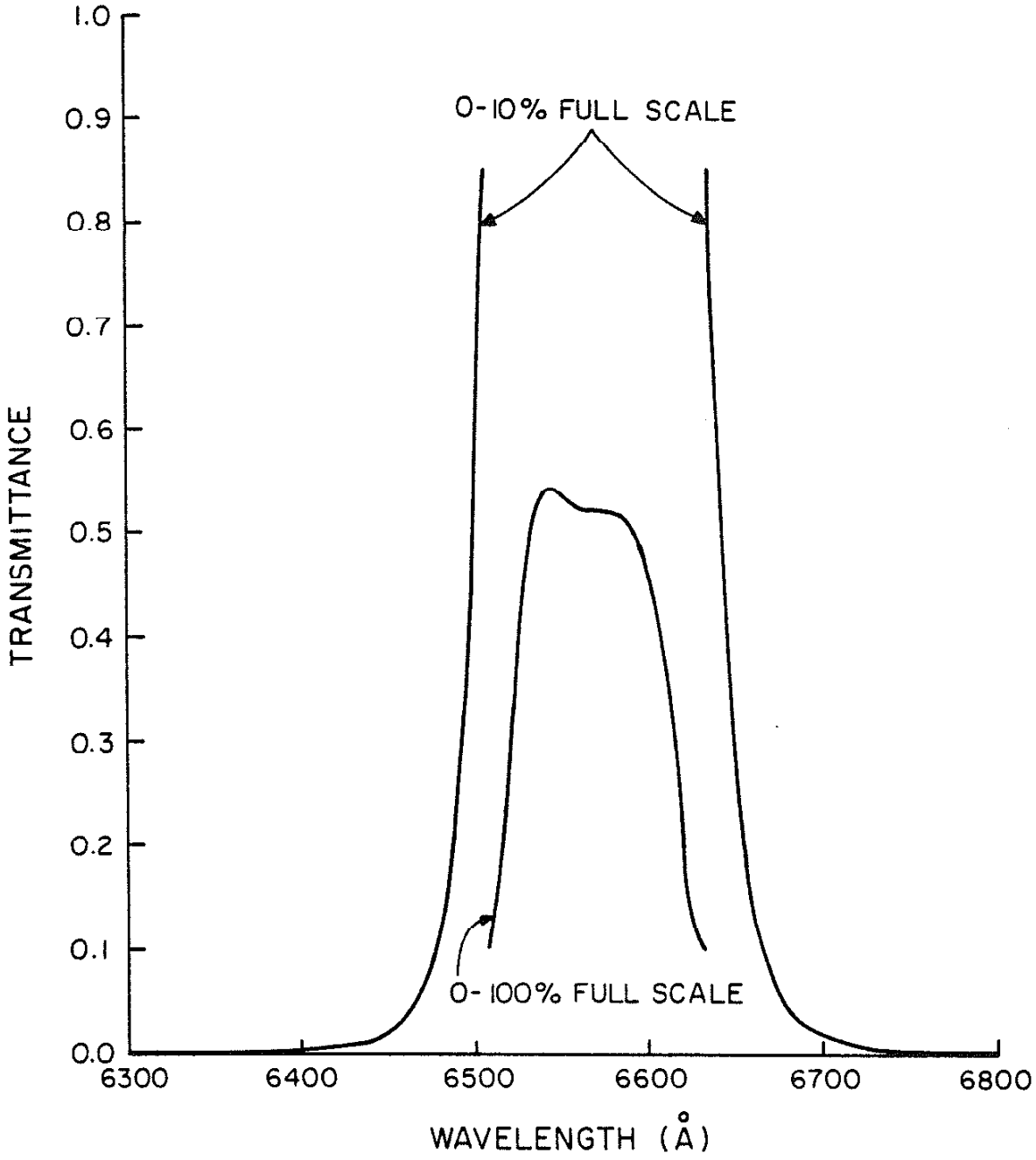

Figure 9. Spectral response of the 6563 Å hydrogen filter.

systems, the normalized spectra were convolved with a Gaussian filter function which closely approximates the actual spectral response of an interference filter. The convolved spectra give the arc power that would be measured through an interference filter. This is given by

$$A_s L_a(\lambda_c) = A_s \int L_a(\lambda)\ F_G(\lambda - \lambda_c)\ d\lambda \quad . \tag{15}$$

$F_G(\lambda)$ is the Gaussian filter function and λ_c is its center wavelength. The filter function is

$$F_G(\lambda) = e^{-(\lambda-\lambda_c)^2/2\sigma^2} \quad , \tag{16}$$

where $\sigma = \dfrac{\text{FWHM}}{2\sqrt{2\ \ell n\ 2}}$.

Note that the Gaussian filter function has unity peak transmittance. The convolved spectra must be multiplied by the peak transmittance of the actual interference filter to be used.

3.4 The Arc Spectra

Plots of the normalized spectra and convolved spectra are shown in Figures 10 through 19. Figures 10 through 14 are spectra obtained using Ar-O_2 shield gas with solid wire and the corresponding convolved spectra. Figures 15 through 19 are for CO_2 shield gas with flux cored wire. All spectra were taken with the welding parameters given in section 3.1. The normalized spectra are plots of the spectral radiant intensity of the arc measured in W/sr·Å versus wavelength in Å. The convolved spectra are plots of the computed radiant intensity of the filtered arc in W/sr versus the center wavelength of the interference filter in Å. Plots of the convolved spectra are for interference filter FWHM bandwidths of 20, 50, and 100 Å.

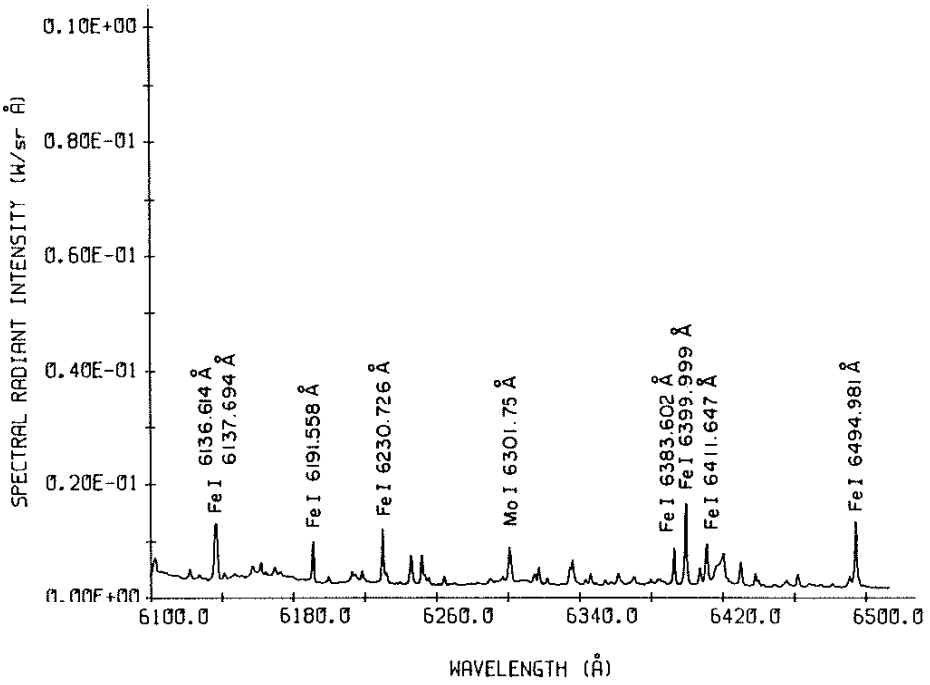

Figure 10a. Normalized weld arc spectra using Ar-O_2 shield gas and solid wire. Wavelength region 6100 - 6500 Å.

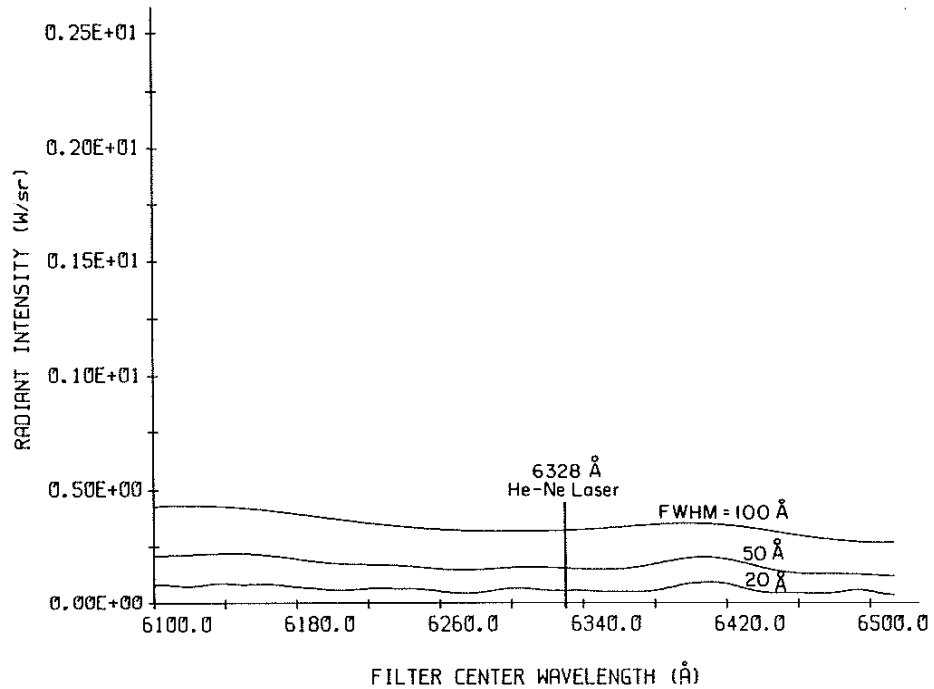

Figure 10b. Filtered weld arc spectra using Ar-O_2 shield gas and solid wire. Wavelength region 6100 - 6500 Å.

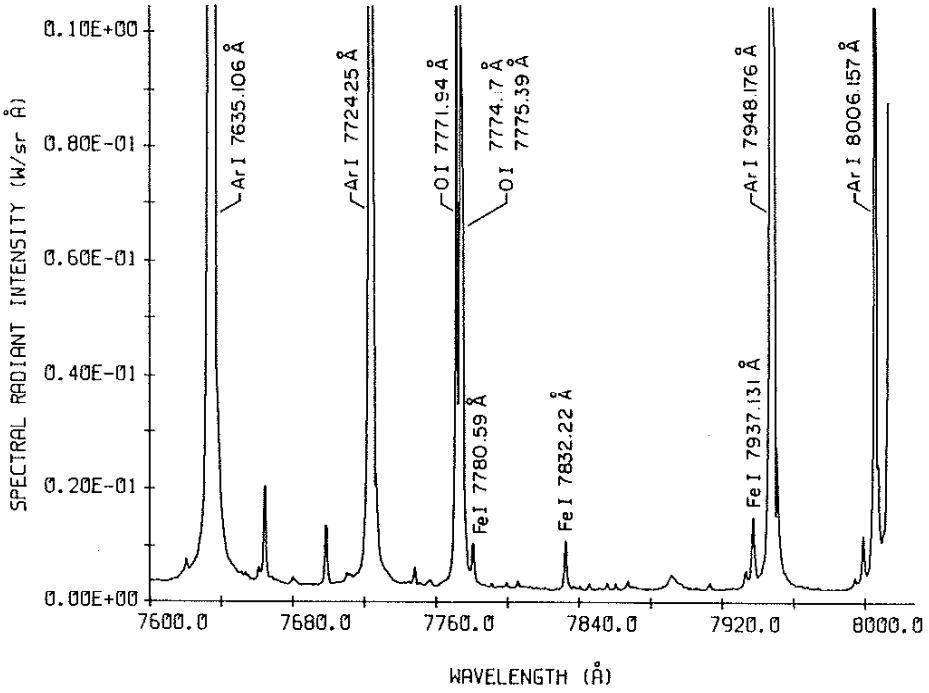

Figure 11a. Normalized weld arc spectra using Ar-O_2 shield gas and solid wire. Wavelength region 7600 - 8000 Å.

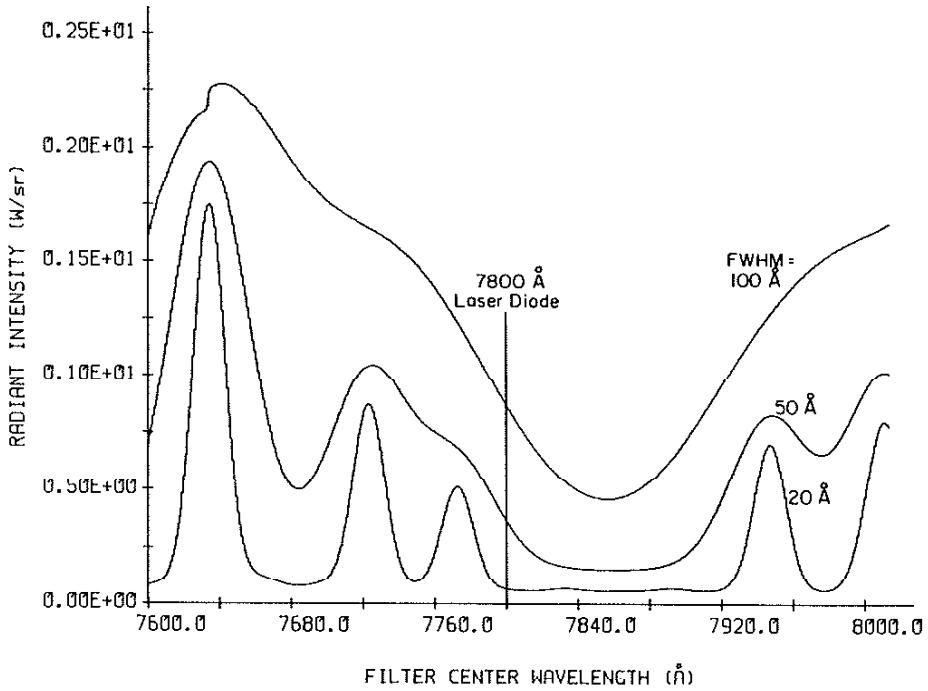

Figure 11b. Filtered weld arc spectra using Ar-O_2 shield gas and solid wire. Wavelength region 7600 - 8000 Å.

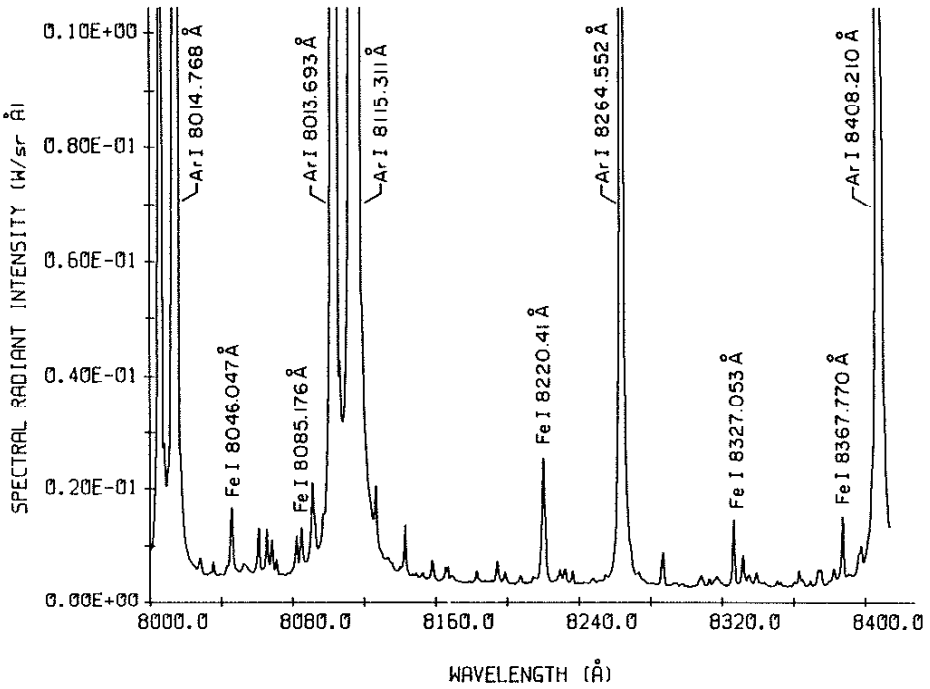

Figure 12a. Normalized weld arc spectra using Ar-0_2 shield gas and solid wire. Wavelength region 8000 - 8400 Å.

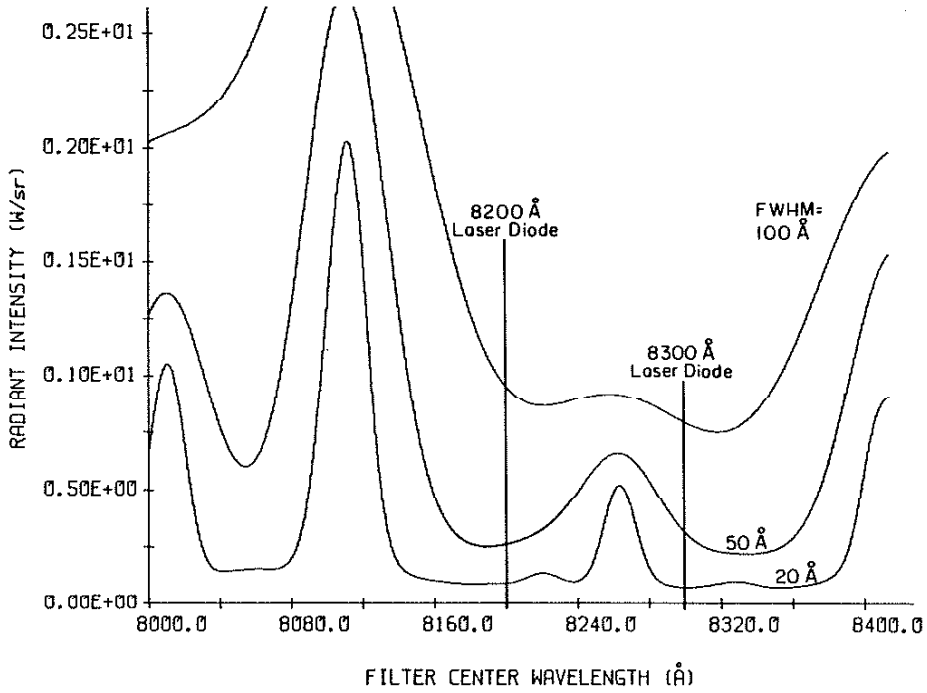

Figure 12b. Filtered weld arc spectra using Ar-0_2 shield gas and solid wire. Wavelength region 8000 - 8400 Å.

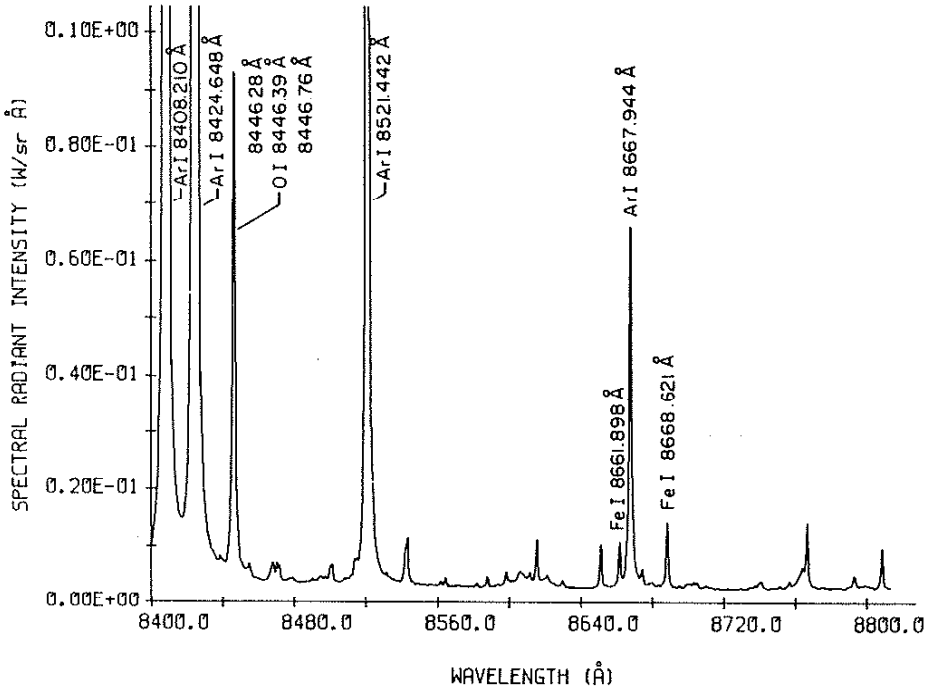

Figure 13a. Normalized weld arc spectra using Ar-0_2 shield gas and solid wire. Wavelength region 8400 - 8800 Å.

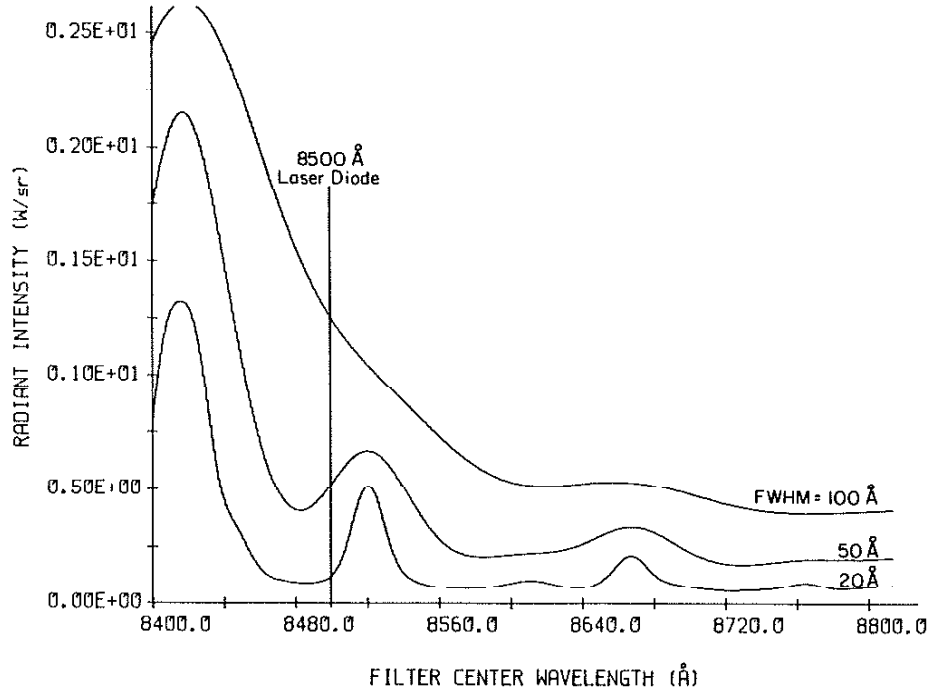

Figure 13b. Filtered weld arc spectra using Ar-0_2 shield gas and solid wire. Wavelength region 8400 - 8800 Å.

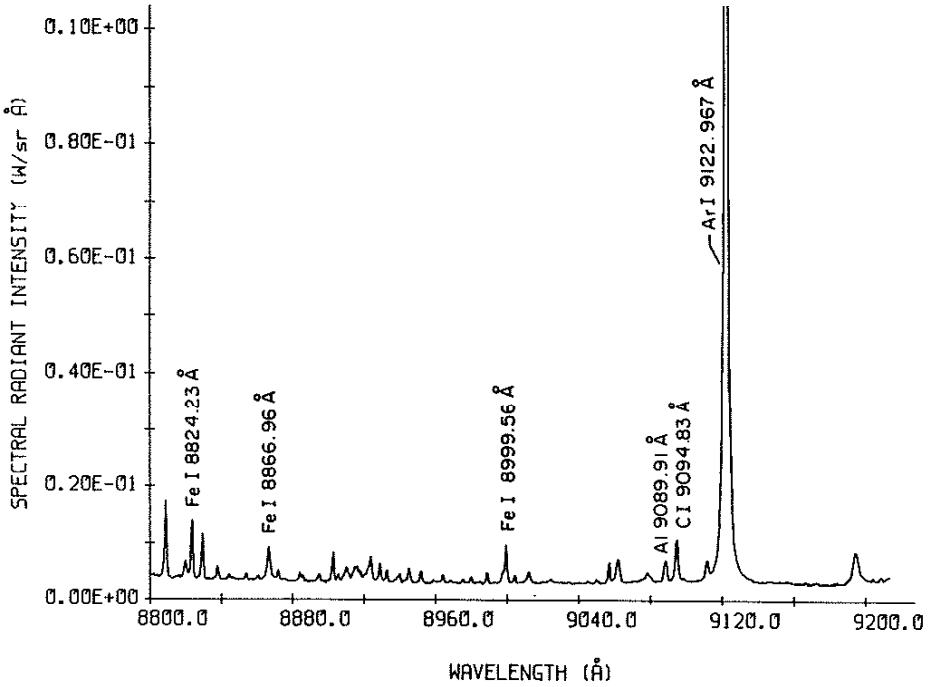

Figure 14a. Normalized weld arc spectra using Ar-O_2 shield gas and solid wire. Wavelength region 8800 - 9200 Å.

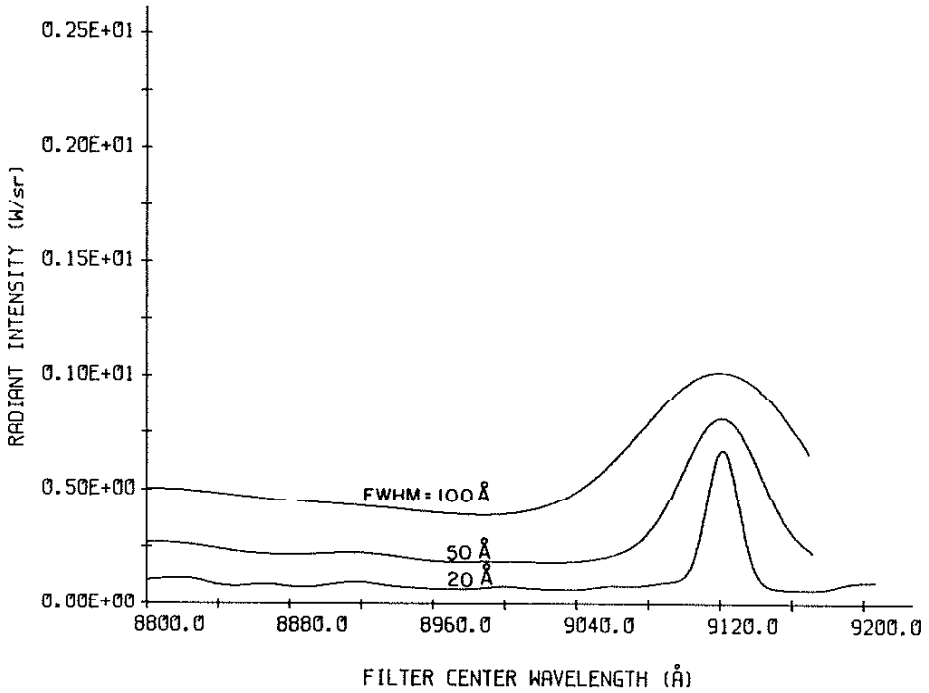

Figure 14b. Filtered weld arc spectra using Ar-O_2 shield gas and solid wire. Wavelength region 8800 - 9200 Å.

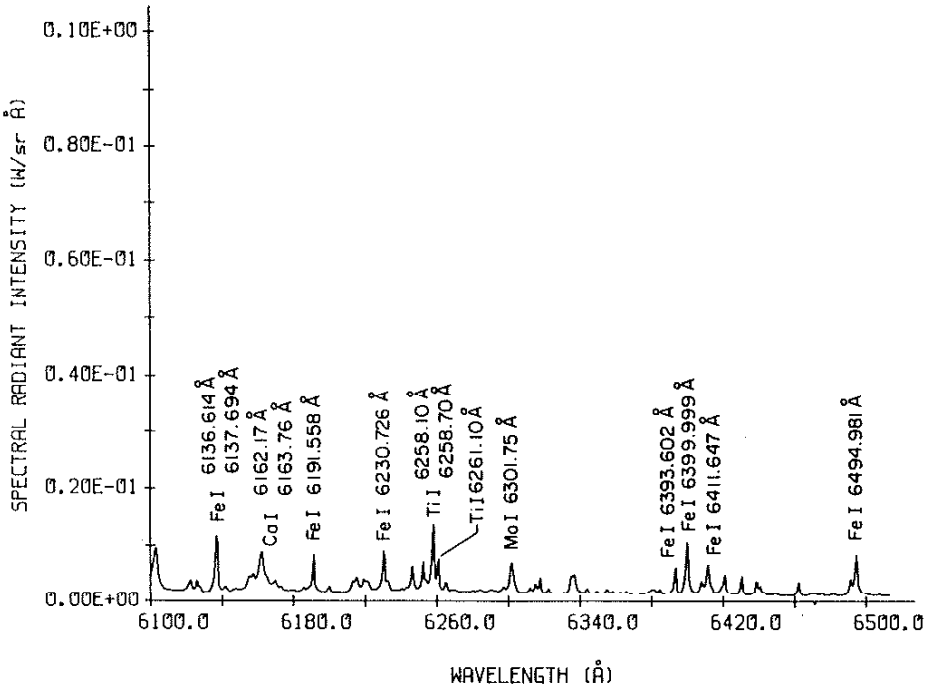

Figure 15a. Normalized weld arc spectra using CO_2 shield gas and flux cored wire. Wavelength region 6100 - 6500 Å.

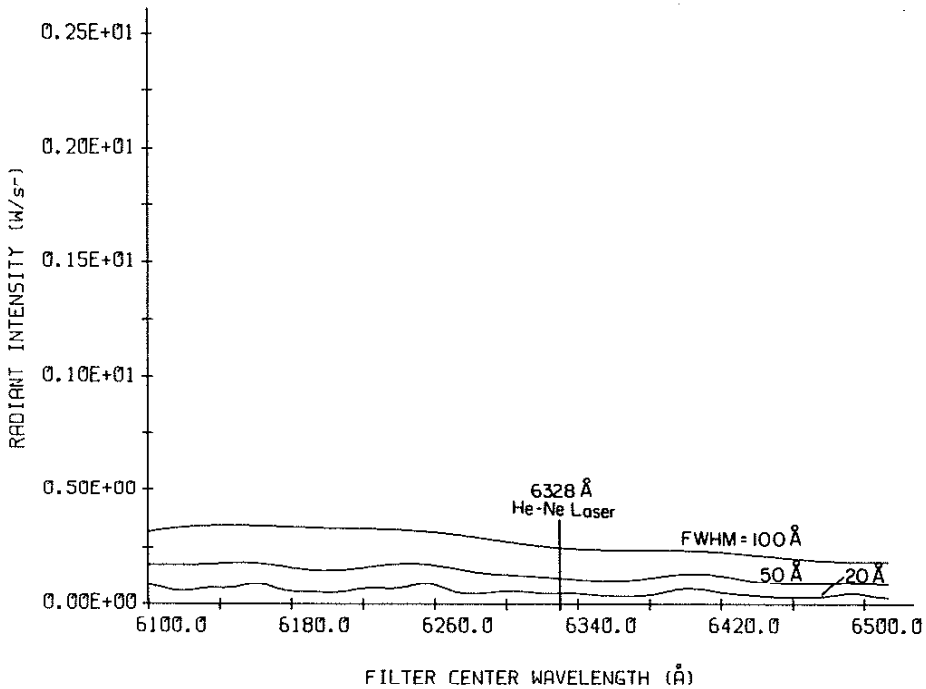

Figure 15b. Filtered weld arc spectra using CO_2 shield gas and flux cored wire. Wavelength region 6100 - 6500 Å.

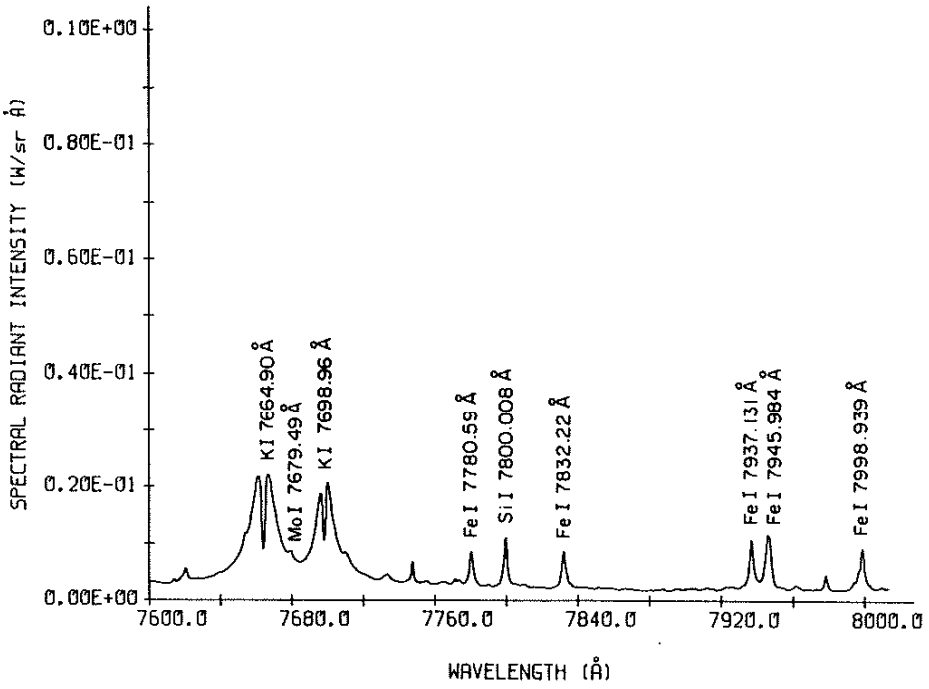

Figure 16a. Normalized weld arc spectra using CO_2 shield gas and flux cored wire. Wavelength region 7600 - 8000 Å.

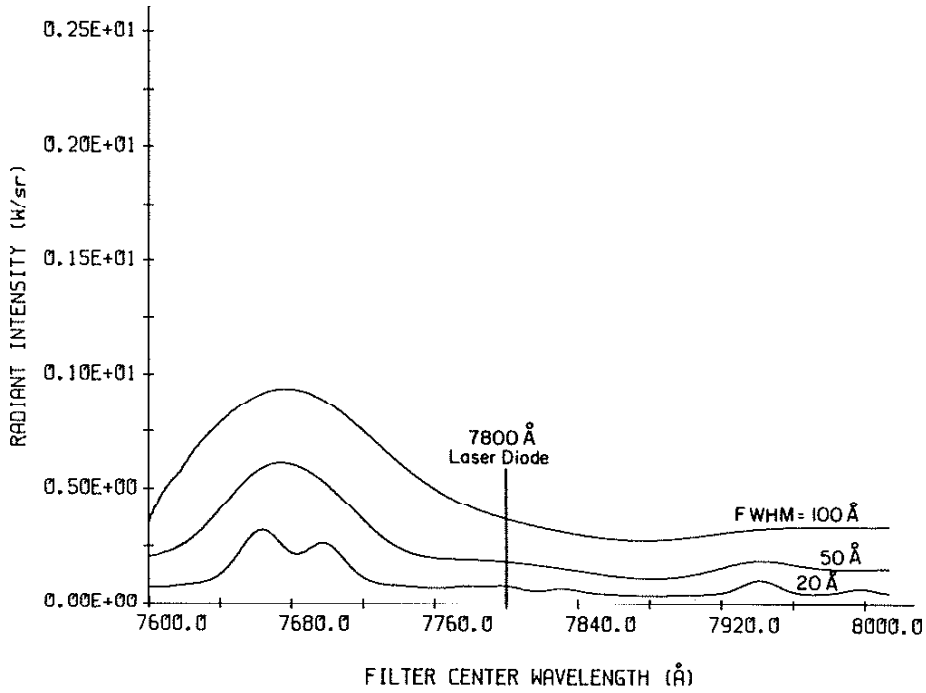

Figure 16b. Filtered weld arc spectra using CO_2 shield gas and flux cored wire. Wavelength region 7600 - 8000 Å.

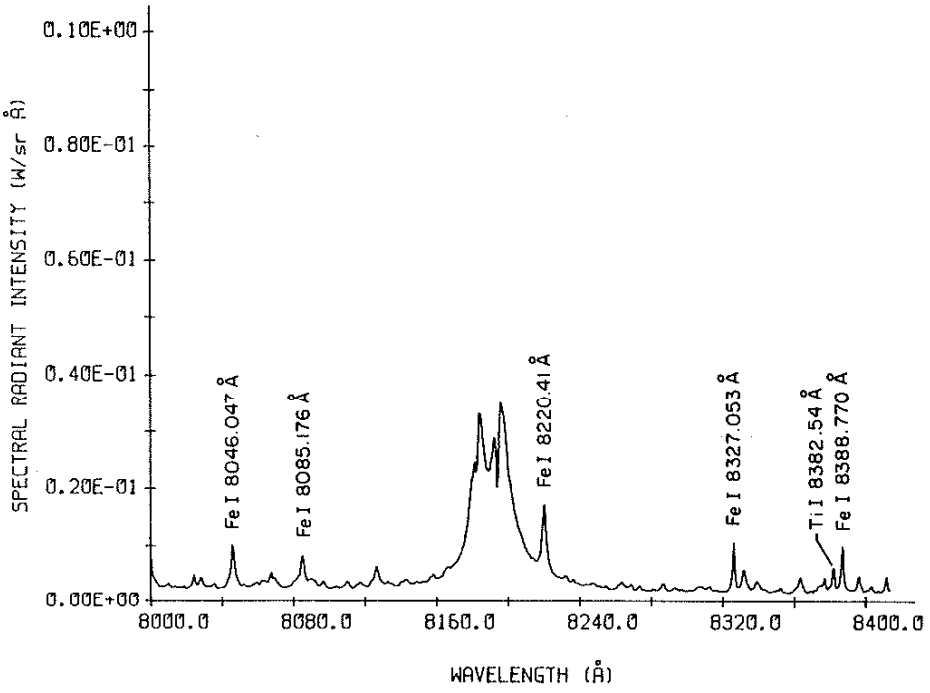

Figure 17a. Normalized weld arc spectra using CO_2 shield gas and flux cored wire. Wavelength region 8000 - 8400 Å.

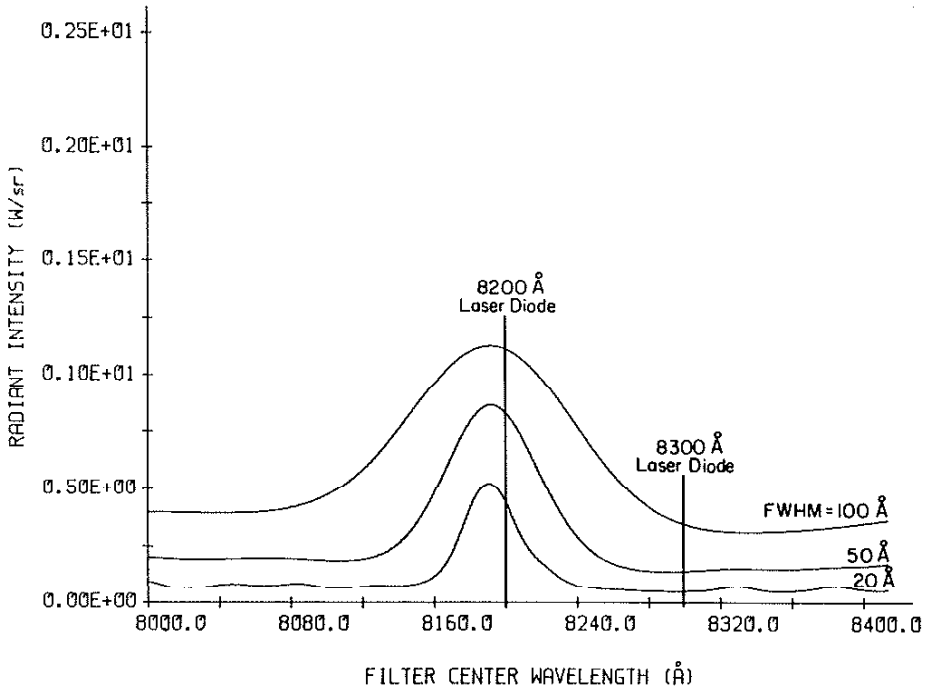

Figure 17b. Filtered weld arc spectra using CO_2 shield gas and flux cored wire. Wavelength region 8000 - 8400 Å.

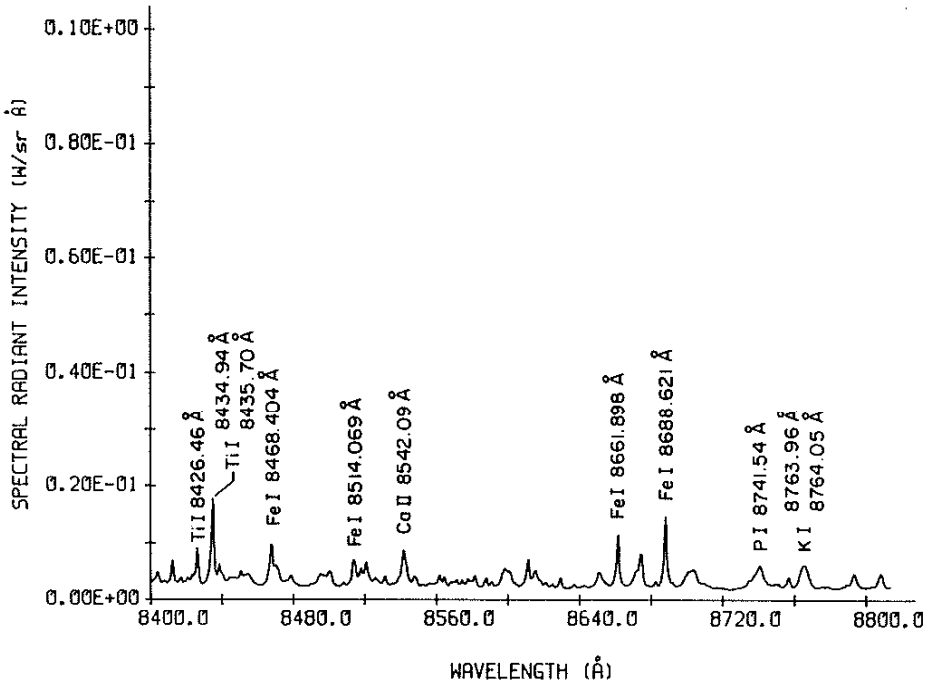

Figure 18a. Normalized weld arc spectra using CO_2 shield gas and flux cored wire. Wavelength region 8400 - 8800 Å.

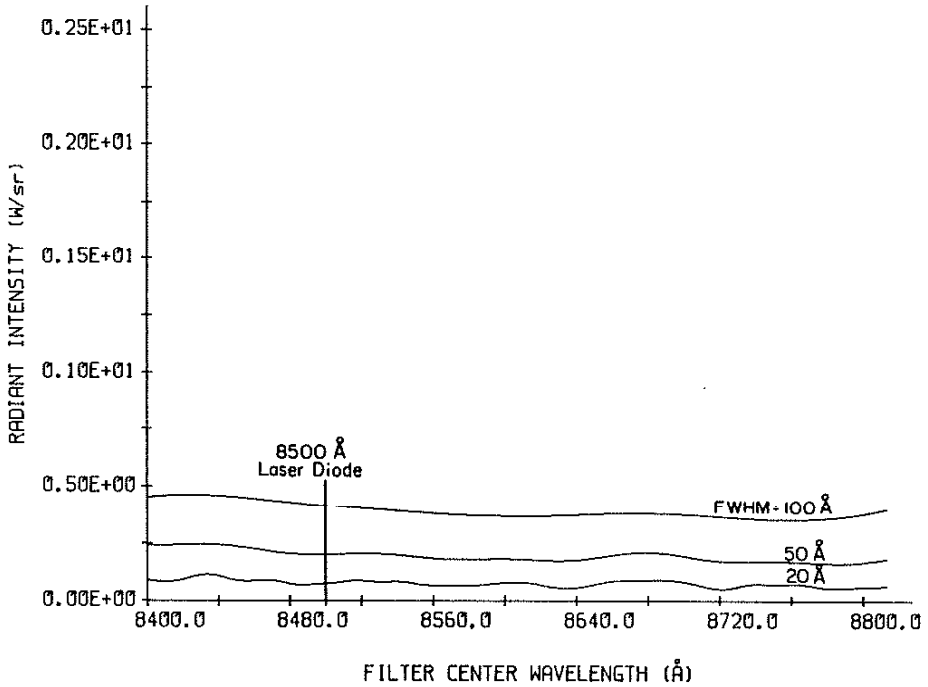

Figure 18b. Filtered weld arc spectra using CO_2 shield gas and flux cored wire. Wavelength region 8400 - 8800 Å.

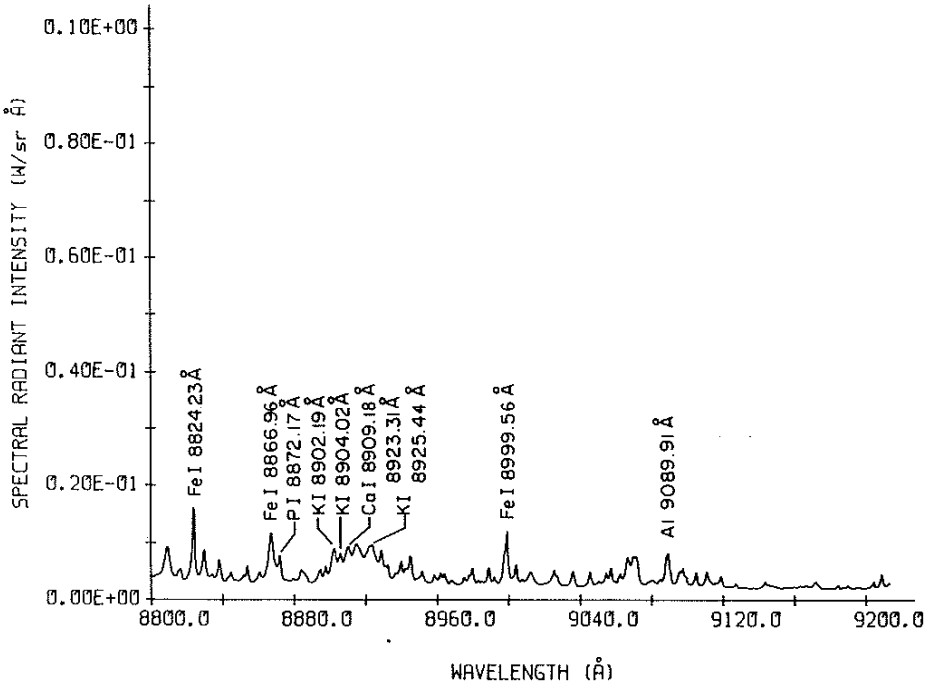

Figure 19a. Normalized weld arc spectra using CO_2 shield gas and flux cored wire. Wavelength region 8800 - 9200 Å.

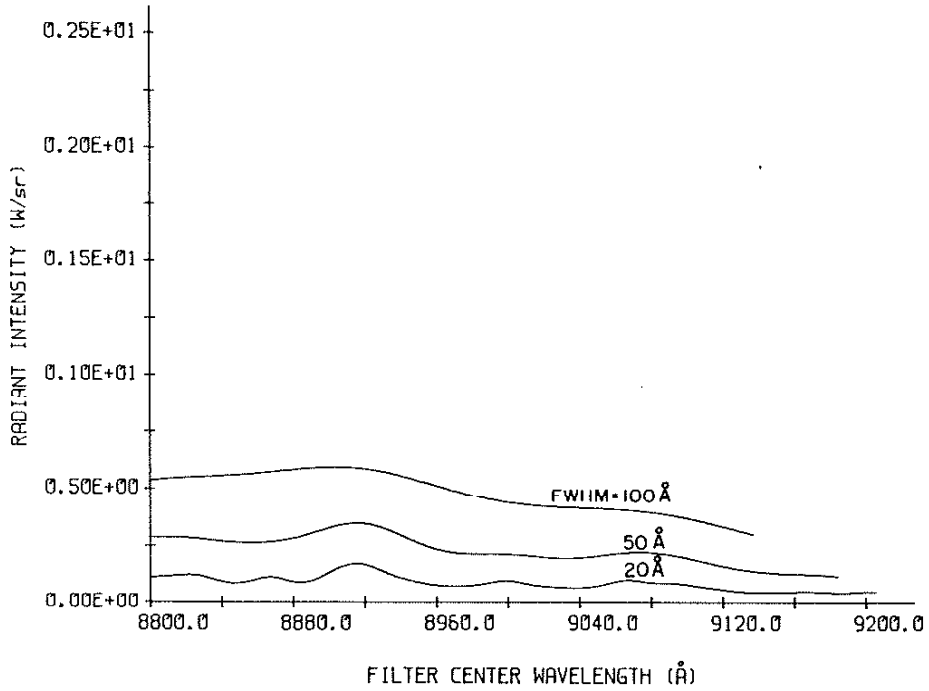

Figure 19b. Filtered weld arc spectra using CO_2 shield gas and flux cored wire. Wavelength region 8800 - 9200 Å.

The convolved spectra have tick marks at common laser diode wavelengths and the 6328 Å He-Ne laser wavelength. Note that the endpoints of the convolved spectra often do not coincide exactly. These differences resulted from variations in the overall arc intensity as the experiment proceeded and are also apparent in the unconvolved spectra. Fluctuations in the compositions of the base metal and electrode wire, arc instability, and other factors may have contributed to the intensity variations which occurred during the experiment.

The spectra in Figures 10a through 19a consist of both discrete spectral line emissions and a continuous background emission. The line emission spectra are primarly from neutral and singly ionized atoms. Disassociation is almost complete in the arc plasma (> 90%) so that nearly all transitions are atomic [15]. The continuous background radiation is blackbody radiation from the hot arc.

The weld arc spectra obtained with the Ar-O_2 and CO_2 shield gases have several obvious and distinctly different features. The high intensity lines in the Ar-O_2 shield gas spectra are all Ar emissions and have narrow line widths. As evident from the convolved Ar-O_2 shield gas spectra, these emissions can produce a significant amount of energy. The other lines, mostly Fe, are not significantly above the continuous background radiation. The CO_2 shield gas spectra contain primarly Fe and Ti lines. Surprisingly, the CO_2 shield gas spectra have a notable absence of O and C lines, even where they are evident in the Ar-O_2 shield gas spectra (Figures 13a and 14a). In the 6100 - 6500 Å spectral region, both the Ar-O_2 and CO_2 shield gas spectra are nearly identical because of the absence of the strong Ar lines. The broad lines present in the CO_2 shield gas spectra (7640 - 7700Å)

are likely to be Stark broadened K emissions due to the flux. Similar emissions, which have not been accurately identified, also occur in the 8160 - 8200 Å region. These lines, like the Ar lines, contribute a significant amount of energy to the spectrum and dominate the filtered arc radiation over large ranges of center wavelengths. Even with a 20 Å filter, this range is close to 100 Å in the CO_2 shield gas spectra and close to 50 Å in the Ar-O_2 shield gas spectra. What is particularly important is that even trace elements in the flux or electrode wire can make large contributions to the arc radiance.

Note that the background radiation in the Ar-O_2 shield gas spectra is somewhat larger than in the CO_2 shield gas spectra throughout the visible red and much of the IR. This is important because the center wavelength of the interference filter should be in a spectral region consisting primarly of background radiation. Thus the illumination of the filtered arc would be greater using Ar-O_2 shield gas than for CO_2. The greater intensity of the background radiation in the Ar-O_2 shield gas spectra is probably an indication of a higher plasma temperature. The intensities of many spectral line emissions are also greater in the Ar-O_2 shield gas spectra, particularly the prominent 6400 Å and 8220 Å Fe lines. This is also an indication of a higher plasma temperature when using Ar-O_2 shield gas since line intensity increases with temperature in accordance with the Boltzmann distribution (see section 3.5).

The continuous background radiation from the arc region can be estimated by the Planck function for blackbodies. To account for the fact that real radiating bodies are not perfect absorbers, the Planck function can be modified to include the emissivity of the radiating body. The

spectral radiant intensity of a radiating body is given by

$$I(\lambda) = A_s L(\lambda) = A_s \varepsilon(\lambda) \frac{2hc^2}{\lambda^5 (e^{hc/\lambda kT} - 1)} , \qquad (17)$$

where $\varepsilon(\lambda)$ = emissivity of radiating body

h = Plancks constant (6.63×10^{-34} J/s)

c = speed of light

k = Boltzmann's constant (1.38×10^{-23} J/K).

If the emissivity is constant, the wavelength of maximum spectral radiant intensity can be computed from

$$(\lambda T)_{peak} = 2898 \ \mu m \ k \qquad (18)$$

To estimate the spectral radiant intensity of the weld arc plasma, we will assume its emissivity is between 0.001 and 0.01, which are the values assumed by Rider [16]. With a source area of 0.5 cm^2 and an assumed arc plasma temperature of 10^4K, the computed spectral radiant intensity of the plasma at 6100 Å is between 0.73 mW/sr·Å to 7.3 mW/sr·Å, depending on the assumed emissivity. The measured background radiation in the spectral data plotted in Figure 10a is 2.8 mW/sr·Å at 6120 Å for the Ar-O_2 weld arc plasma and 2.2 mW/sr·Å at 6115 Å for the CO_2 weld arc plasma. These figures are comparable to the blackbody estimate.

The background radiation in the arc region can be attributed to the arc plasma, molten droplets in the arc, and possibly to the molten weldpool. Figures 20, 21, and 22 are plots of the Planck function for temperatures normally associated with an Ar-O_2 weld arc plasma, the metal droplets, and the molten weldpool. They are plots of the relative spectral radiant intensity over small ranges of temperatures versus wavelength in Å. The

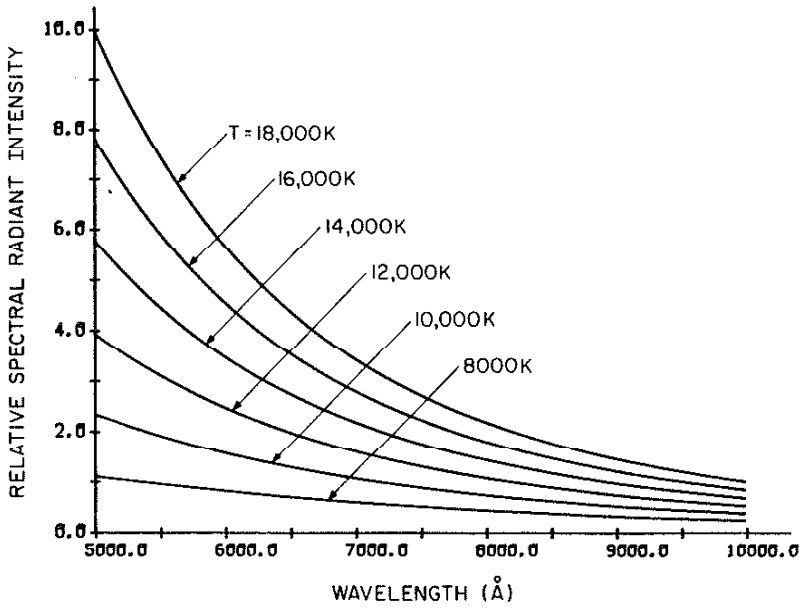

Figure 20. Blackbody radiation from weld arc plasma. Temperatures range from 8000 - 18,000K.

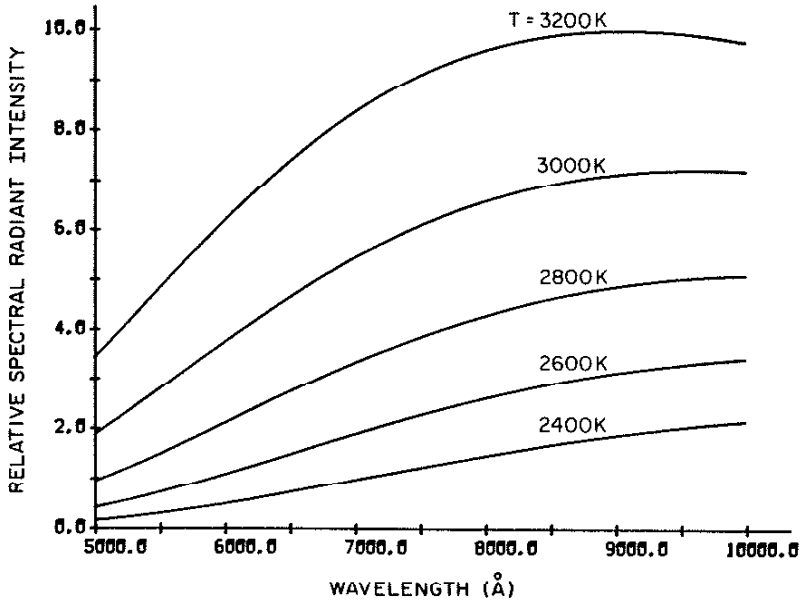

Figure 21. Blackbody radiation from molten droplets in the arc region. Temperatures range from 2400 - 3200K.

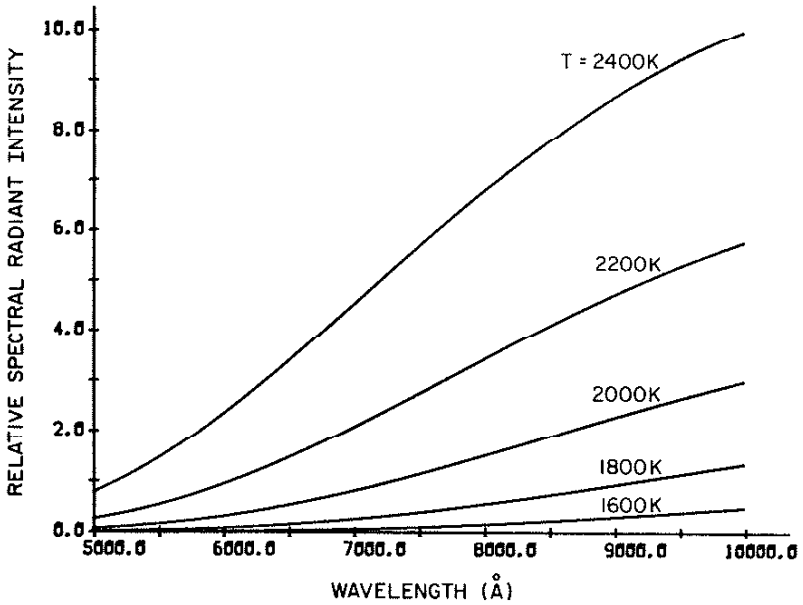

Figure 22. Blackbody radiation from the molten weldpool. Temperatures range from 1600 - 2400K.

curves indicate expected trends in the continuous background radiation of the arc plasma and of molten steel, assuming a constant emissivity. The arc plasma temperatures are similar to those measured by Kobayashi and Suga for a 100 A, 15 V gas-tungsten arc (GTA) with Ar shield gas using spectrographic methods [17]. Measurements by Ludwig [14] for a 300 A GTA are comparable. Droplet temperatures measured by Heiro and North approached 2800K in a GMA [18]. All these investigations are discussed in Milton [11]. Milton also discusses experimental and theoretical estimates of the weldpool temperature for steel from several investigators. Estimates are between 1700K and about 2400K [19-21].

Note that the radiation from the arc plasma is significant near the UV while radiation from the cooler bodies such as the molten droplets is large in the near IR because of the shift in the maximum (Eq. (18)). Furthermore, these trends are present over a wide range of possible arc plasma temperatures and molten steel temperatures. Thus wavelengths shorter than 6000 Å and longer than 9000 Å should probably be avoided in the operation of vision systems.

Because of the large intensity fluctuations of the arc, the spectral data does not indicate which source of blackbody radiation predominates in the near IR. However, both the Ar and CO_2 shield gas spectra show an increase in background radiation towards the shorter wavelengths in the visible red (see Figure 23), indicative of the expected blackbody curve for the arc plasma shown in Figure 20.

3.5 Effect of Different Welding Conditions on Line Emission Spectra

Welding conditions in typical GMA applications are extremely varied,

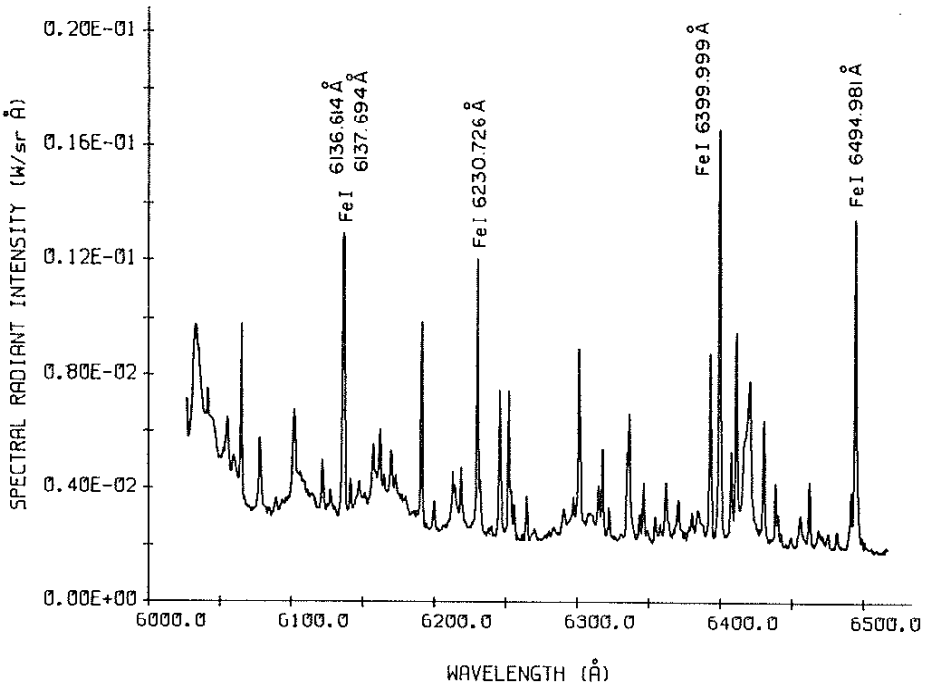

Figure 23a. Normalized weld arc spectra using Ar-O_2 shield gas and solid wire. Wavelength region 6000 - 6500 Å. Enlarged to show increased background radiation near 6100 Å.

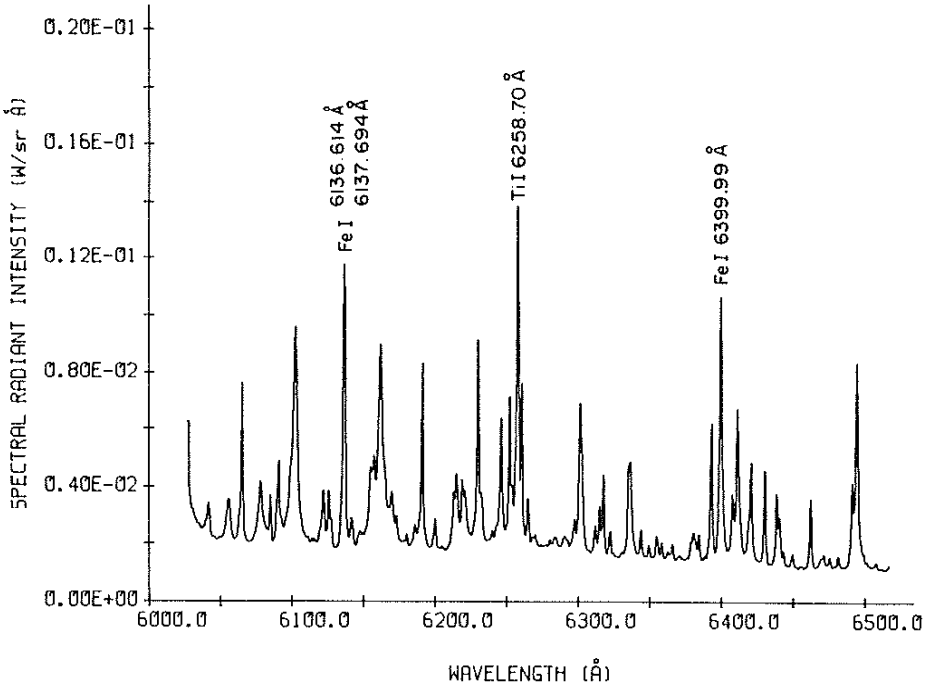

Figure 23b. Normalized weld arc spectra using CO_2 shield gas and flux cored wire. Wavelength region 6000 - 6500 Å. Enlarged to show increased background radiation near 6100 Å.

depending upon the shield gas mixture, electrode wire and base metal compositions, and the welding parameters. Under such varied conditions, the spectral data presented here cannot be expected to accurately represent the actual intensity of spectral line emissions from the arc plasma in all situations. However, relative intensities of line emissions depend almost entirely on the arc plasma temperature and its composition. In many welding applications, the arc plasma will have temperatures and compositions similar to those of the experiment so that the spectral emissions should also be similar, even though the absolute intensities may be different. For the purpose of choosing favorable center wavelengths for lasers and interference filters, the relative intensities should be adequate.

Literature which discusses the effect of the welding parameters and composition of welding materials on the arc temperature appears to be very sparse, particularly for the case of the GMA. Although applied to the GTA, some of the theoretical work by Ramakrishnan and Nuon [22] and experimental work of Kobayisha and Suga [17] may be useful. Their results indicate that the arc temperature increases when the current is increased or the voltage is decreased. Ramakrishnan and Nuon also report that the arc column properties such as temperature, arc radius, and column voltage show only a weak dependence on the cathode spot size. This adds impetus for predicting trends in temperature of the GMA based upon the GTA. In GTA welding, the cathode spot size is determined by the size of the electrode tip. However, there is no such constraining factor in GMA welding because the cathode is on the workpiece.

The relative intensity of a spectral line can be determined by the Boltzmann distribution:

$$S = ng_i A_{ij} \frac{hc}{\lambda} \frac{e^{-E_i/kT}}{Z(T)} \qquad (19)$$

where S = relative spectral line intensity

n = density of constituent

g_i = degeneracy of i^{th} state

A_{ij} = transition probabilty

E = excitation energy

$Z(T)$ = partition function.

The partition function is a slowly varying function of temperature at the elevated arc plasma temperatures. Thus if the excitation energy of the i^{th} state is on the order of KT and the transition probabilty is not too small, the spectral line will appear in the spectra. Increasing the temperature results in more spectral lines appearing as well as increasing the strength of lines already present in the spectra. Decreasing the temperature has the opposite effect.

Predicting whether changes in the composition of the base metal and electrode alloys, shield gas, and flux will introduce strong emission lines into the weld arc spectra is very difficult. Very strong emissions produced in the hot arc column can be absorbed in the cooler regions in the immediate vicinity of the arc. Furthermore, the composition of the arc depends upon the vapor pressures of elements which compose the base metal and electrode alloys [23]. However, there are some useful guidelines for determining whether a particular element will produce strong spectral emissions. For any given species, the relative intensities of line emissions will depend upon the transition probabilities and excitation energies for a given

transition. The intensity of spectral emissions from a given species will be proportional to the total number of atoms of that species in the arc plasma if absorption is neglected. It may also be useful to compare the relative proportions of elements in one of the alloys, the shield gas mixture, or the flux. The comparison should be made between elements which have similar chemical properties. If one of these elements were present in the experiment and produced recognizable spectral emissions, Equation (19) could be used as a basis of comparison by neglecting the partition functions. An assumed temperature of 10^4K would be suitable. A good source of spectroscopic data is the National Bureau of Standards, Wavelengths and Transition Probabilities for Atoms and Atomic Ions [24]. Further information on spectroscopic methods as applied to weld arcs can be found in Mills [23] and Shea and Gardner [25].

4. DESIGN EXAMPLE

To illustrate the use of the spectral measurements, we will consider a simple design example. Table 5 gives the wavelengths and power outputs of some commercially available CW lasers. Referring to Figures 10b through 19b, we find that only the 6328, 7800, and 8300 Å wavelengths are situated in regions of low arc emission for both shield gases. Suppose that the arc is centered 1 cm above the workpiece and the projected pattern is 4 cm from the center of the arc. Light from the arc is incident on the workpiece at about 15°. Substituting the radiant intensity of the filtered arc obtained from the convolved spectra into Equation (6) gives the irradiance of the arc in the vicinity of the pattern. Table 6 shows the results of this calculation for the five wavelengths considered and for filter bandwidths of 20, 50, and 100 Å. This was done for both Ar and CO_2 shield gases. The irradiance of the arc is given in $\mu W/mm^2$. With the exception of the strong spectral emissions in the vicinity of 8200 Å with the CO_2 shield gas, the CO_2 values are typically less than those obtained with Ar shield gas. This is an indication of the lower background radiation of the CO_2 arc noted earlier. As expected, the 8200 and 8500 Å wavelengths are generally undesirable, even with the 20 Å filter. If only CO_2 were intended to be used, the 8500 Å wavelength could yield acceptable results.

Using the laser output powers specified in Table 5, we can compute the SNR. We will assume that the pattern is a stripe 1 mm wide by 20 mm long and illuminates the workpiece normally. The signal-to-noise ratios for the sample lasers listed in Table 5 were computed from Equation (8) and are shown in Table 7. A quick glance indicates that the 8300 Å laser diode is the best performer; of course, its higher power output makes it a rather

TABLE 5

WAVELENGTHS AND POWER OUTPUTS OF

SOME COMMERCIALLY AVAILABLE LASERS

(From Laser Focus Buyer's Guide, 1984 ed., [26])

WAVELENGTH (Å)	POWER (mW @ drive in mA)	MANUFACTURER	MODEL NO.
6328	5	Hughes, IPD	3225H/HP
7800	3 @30	Mitsubishi Electronic	ML-4102
8200	5 @150	RCA Electro-Optics	C86000E
8300	15 @65	Mitsubishi Electronic	ML-5101A
8500	8 @130	NEC Electronics	NDL-3108

5. CONCLUSION

We have presented measurements of the spectral radiant intensity of an arc weld plasma with Ar and CO_2 shield gases. These measurements include the 6328 Å He-Ne laser wavelength and those wavelengths which are typical of near infrared laser diodes. The normalized spectra, when integrated with the appropriate filter function, provide a simple method for estimating the SNR of various hypothetical vision systems. Many wavelengths, including the 8300 Å laser diode wavelength and the 6328 Å He-Ne laser wavelength, appear to be suitable. Filtering of strong line emissions appears to be a problem for the larger bandwidth filters, particularly if more than one shield gas is to be used. However, narrow filter bandwidths can be used if the temperature variations are not too adverse.

APPENDIX A

CATALOGING OF UV AND IR WELD ARC SPECTRA

A.1. The Weld Arc Spectra

In this section, we present UV and IR weld arc spectra from 3150 - 4250 Å and from 7350 - 9950 Å. The cataloging of these spectra expands a previous catalog of weld arc spectra in the visible and near IR spectrum [10]. Welding was performed on ASTM 242 low alloy steel using E70S-3 electrode wire. The shield gas mixture was 98% Ar - 2% O_2. The welding parameters were identical to those described in Section 3.1 with the exception of the travel speed. The travel speed was 15 cm/s. The UV spectra were obtained using a quartz lens and an armoured, Dolan-Jenner quartz fiber optic bundle. A 2400 line/mm holographic grating was used to obtain the UV spectra and provided an overall bandwidth of about 250 Å. The IR spectra were obtained using the glass optics and a 1200 line/mm grating. The optics and the monochromator slit width were adjusted to obtain strong spectra and were frequently changed between data sets.

The UV spectra appear in Figures A.2.1 - A.2.11 and the IR spectra appear in Figures A.3.1 - A.3.13. The parenthetical wavelengths denote second order spectral lines. Their actual wavelengths are one-half the measured wavelengths. There was an occasional problem of diode saturation. The appearance of two peaks in the 8115.311 Å Ar line in Figure A.3.4. was a result of saturation. The 3933.66 Å and 3968.45 Å Ca II emissions in Figures A.2.8 and A.2.9. were unexpected because Ca does not normally occur in ASTM 242 steel or E70S-3 electrode wire. However, their measured wavelengths of 3933.63 Å and 3968.45 Å are nearly exact. They are also the strongest Ca emissions in the UV spectrum [24].

TABLE 6

IRRADIANCE OF FILTERED ARC - EXAMPLE
(For lasers listed in Table 5)

WAVELENGTH (in Å)	IRRADIANCE OF FILTERED ARC (in μW/mm)					
	INTERFERENCE FILTER FWHM					
	20 Å		50 Å		100 Å	
	Ar	CO_2	Ar	CO_2	Ar	CO_2
6328	9.6	7.4	25	19	50	38
7800	11	14	60	29	131	58
8200	14	69	40	130	150	191
8300	12	8.0	48	22	123	54
8500	19	12	81	31	197	64

TABLE 7

COMPUTED SIGNAL-TO-NOISE RATIOS - EXAMPLE
(For lasers listed in Table 5)

WAVELENGTH (in Å)	SIGNAL-TO-NOISE RATIO					
	INTERFERENCE FILTER BANDWIDTH (FWHM)					
	20 Å		50 Å		100 Å	
	Ar	CO_2	Ar	CO_2	Ar	CO_2
6328	26	34	10	13	5.0	6.6
7800	14	11	2.5	5.1	1.1	2.5
8200	18	3.6	6.3	1.9	1.7	1.3
8300	63	94	16	34	6.1	14
8500	21	33	4.9	13	2.0	6.3

expensive device. The He-Ne laser performance is also quite good. In view of the availablity of rugged, relatively low cost He-Ne lasers, the He-Ne laser may be a better choice than the 8300 Å laser diode. The 7800 Å laser diode also has a moderately high SNR. It may be the most cost effective solution on a per watt basis. The 8500 Å laser diode is also acceptable for CO_2 welding. Note that the computed signal-to-noise ratio increases by a factor of r^3 so that less expensive, wider bandwidth interference filters may be suitable at larger distances. Also note that commercially available laser diodes can have almost any wavelength in the near IR by adjusting the lattice composition.

Although using the smallest bandwidth filters available would obviously yield the best SNR, some practical problems arise: (1) the spectral bandwidth of many laser diodes may be larger than the bandwidth of the filter, reducing the available laser output power; (2) the elevated temperatures of the welding environment change the filter center wavelength; and (3), the filter blue shifts as the periphery of the camera FOV is approached. The consideration of the laser diode bandwidth is primarly one of cost since laser diodes with narrow spectral bandwidths (<10 Å) are commonly available. To appreciate the other factors, consider an example using a Melles-Griot interference filter (model no. 03 FIL 006) with a 10 Å bandwidth and centered at 6328 Å [27]. If the temperature is 75°C, the change in center wavelength from the ambient value at 20°C is about +15 Å. If the FOV of the camera is 25 mm by 25 mm and the camera is situated 100 mm from the workpiece, the maximum angle of incidence is 0.13 rad. This corresponds to a change in the center wavelength of about -11 Å. Thus both temperature and spatial variations can shift the center wavelength beyond

the 10 Å bandwidth. Consequently, a filter with a bandwidth larger than 10 Å must be used.

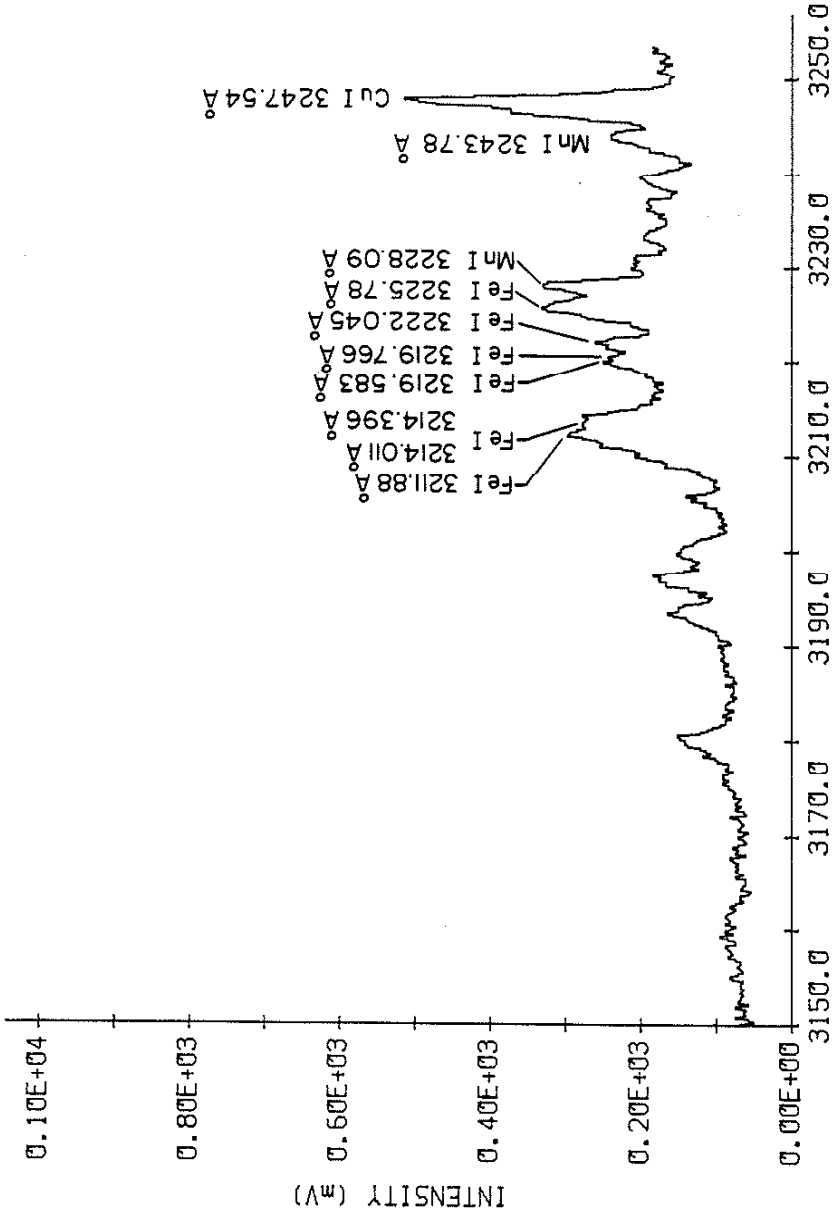

Figure A.2.1. Weld arc spectra using Ar-O_2 shield gas and solid wire. Wavelength region 3150 - 3250 Å.

A.2. Catalog of UV Spectra from 3150 - 4250 Å

Wavelengths (Å)	Filename
3150 - 3250	ALW060
3250 - 3350	ALW034
3350 - 3450	ALW034
3450 - 3550	ALW063
3550 - 3650	ALW063
3650 - 3750	ALW064
3750 - 3850	ALW064
3850 - 3950	ALW065
3950 - 4050	ALW065
4050 - 4150	ALW043
4150 - 4250	ALW043

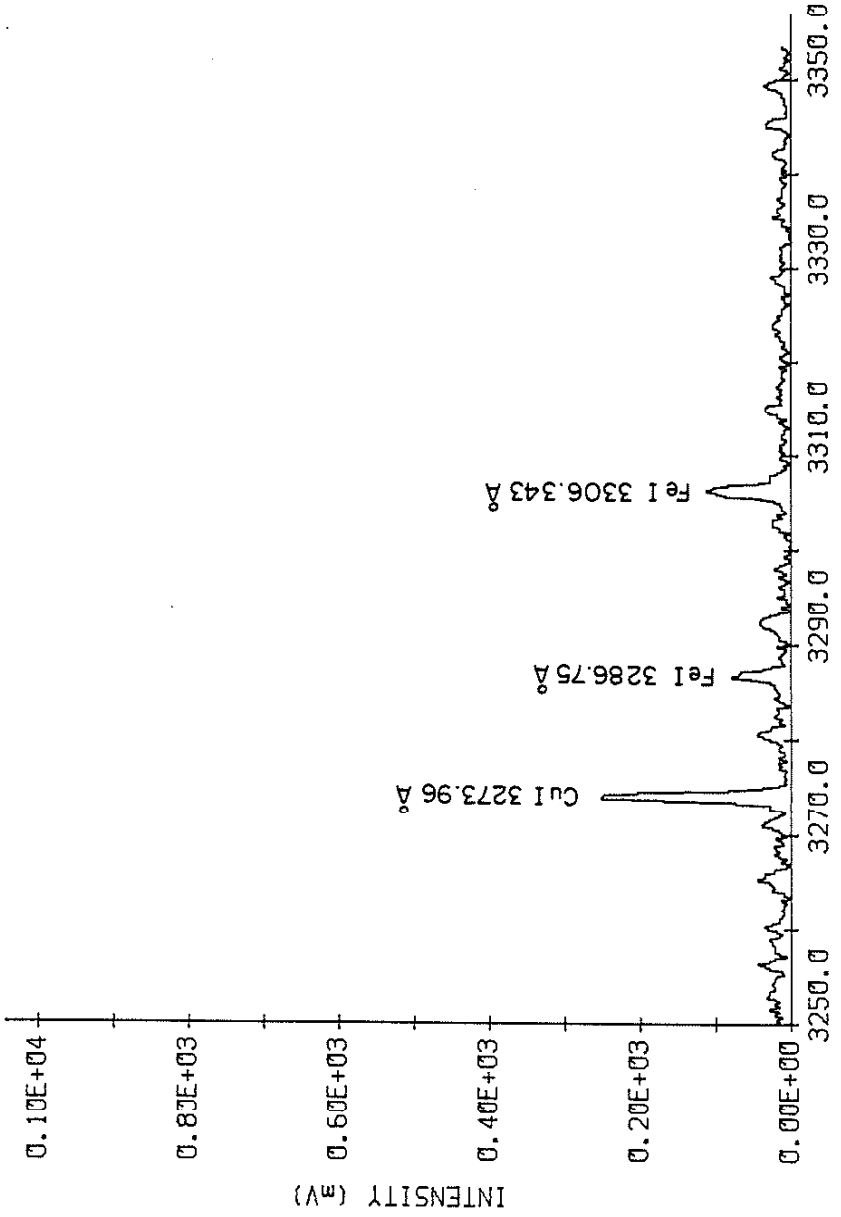

Figure A.2.2. Weld arc spectra using Ar-O_2 shield gas and solid wire. Wavelength region 3250 - 3350 Å.

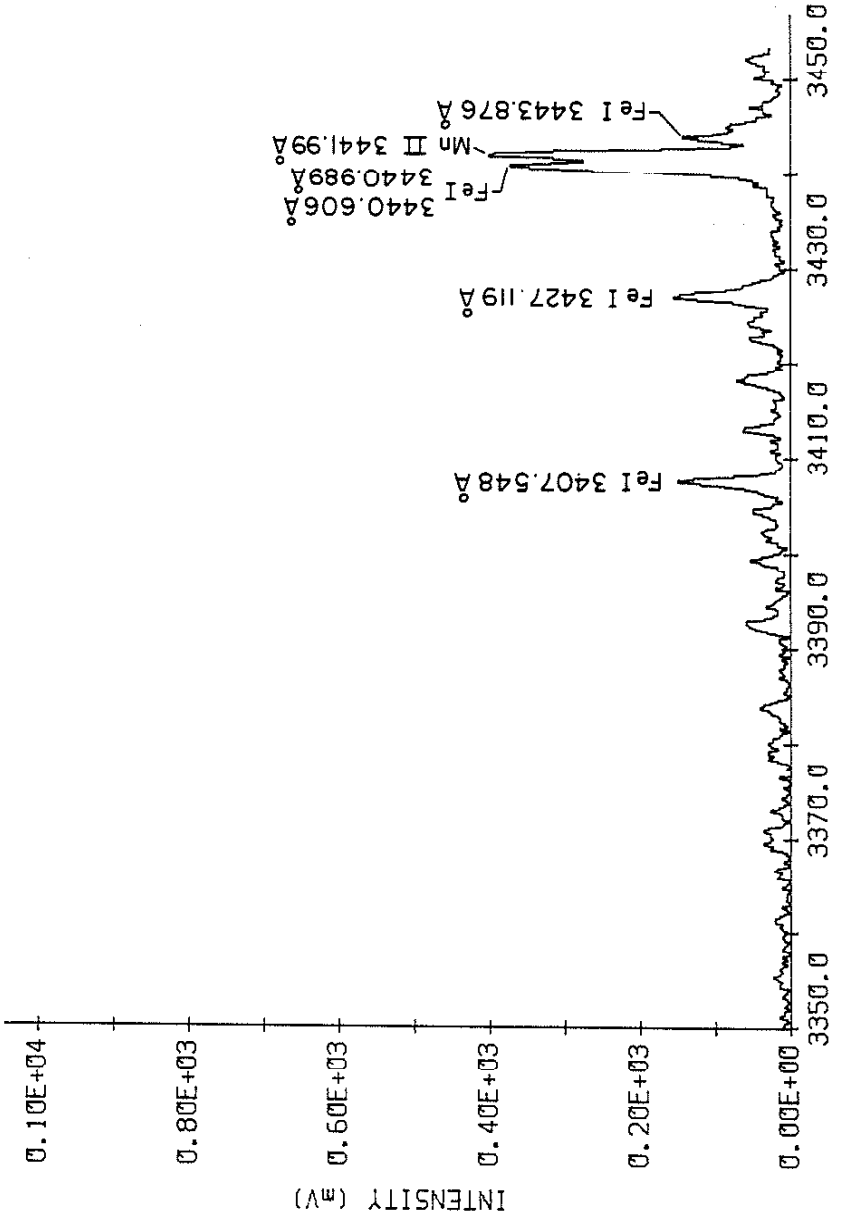

Figure A.2.3. Weld arc spectra using Ar-O_2 shield gas and solid wire. Wavelength region 3350 - 3450 Å.

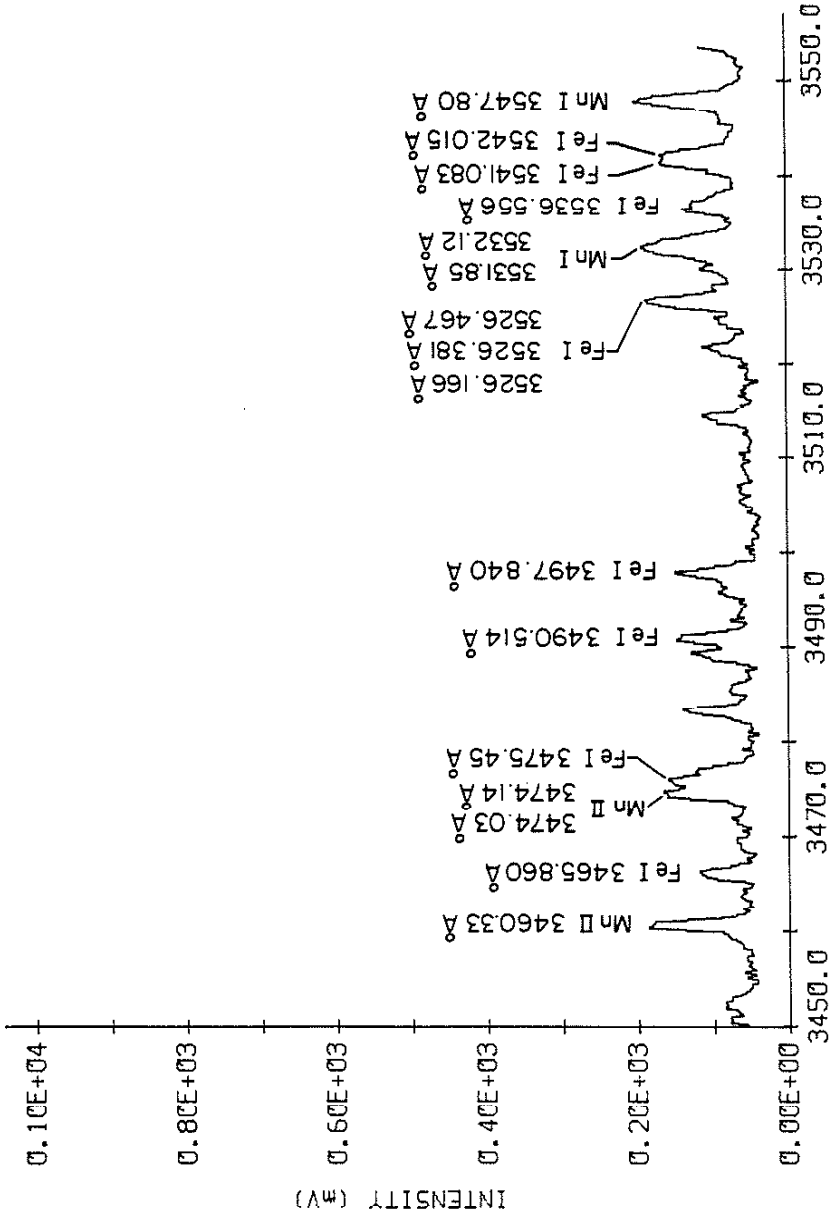

Figure A.2.4. Weld arc spectra using Ar-0_2 shield gas and solid wire. Wavelength region 3450 - 3550 Å.

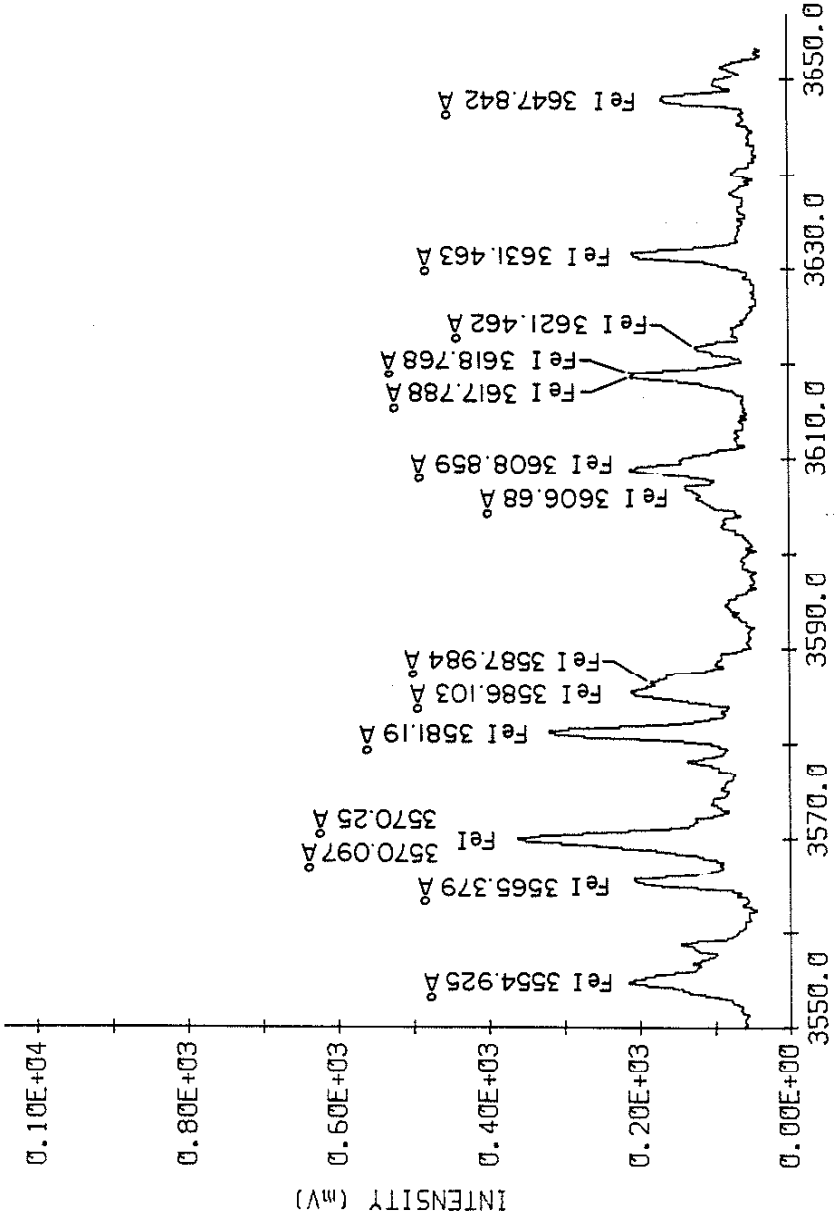

Figure A.2.5. Weld arc spectra using Ar-O_2 shield gas and solid wire. Wavelength region 3550 - 3650 Å.

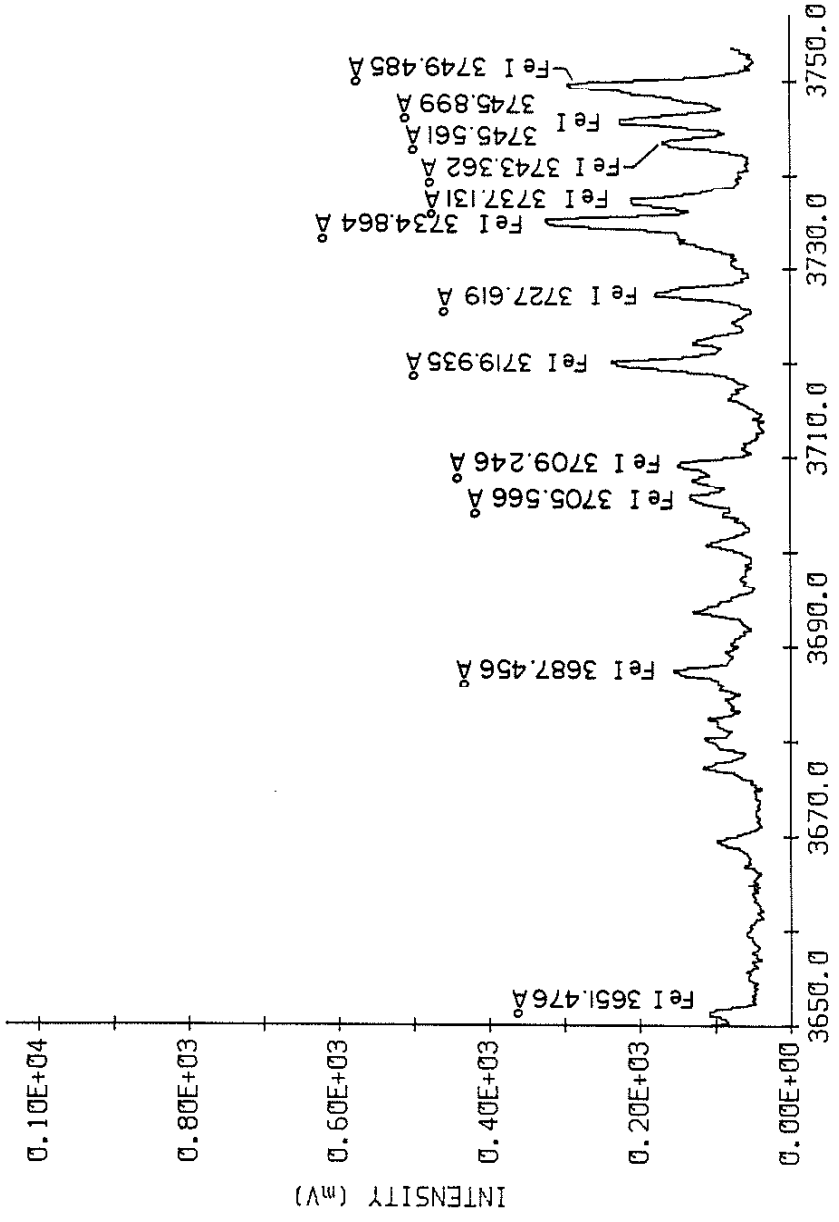

Figure A.2.6. Weld arc spectra using Ar-O_2 shield gas and solid wire. Wavelength region 3650 - 3750 Å.

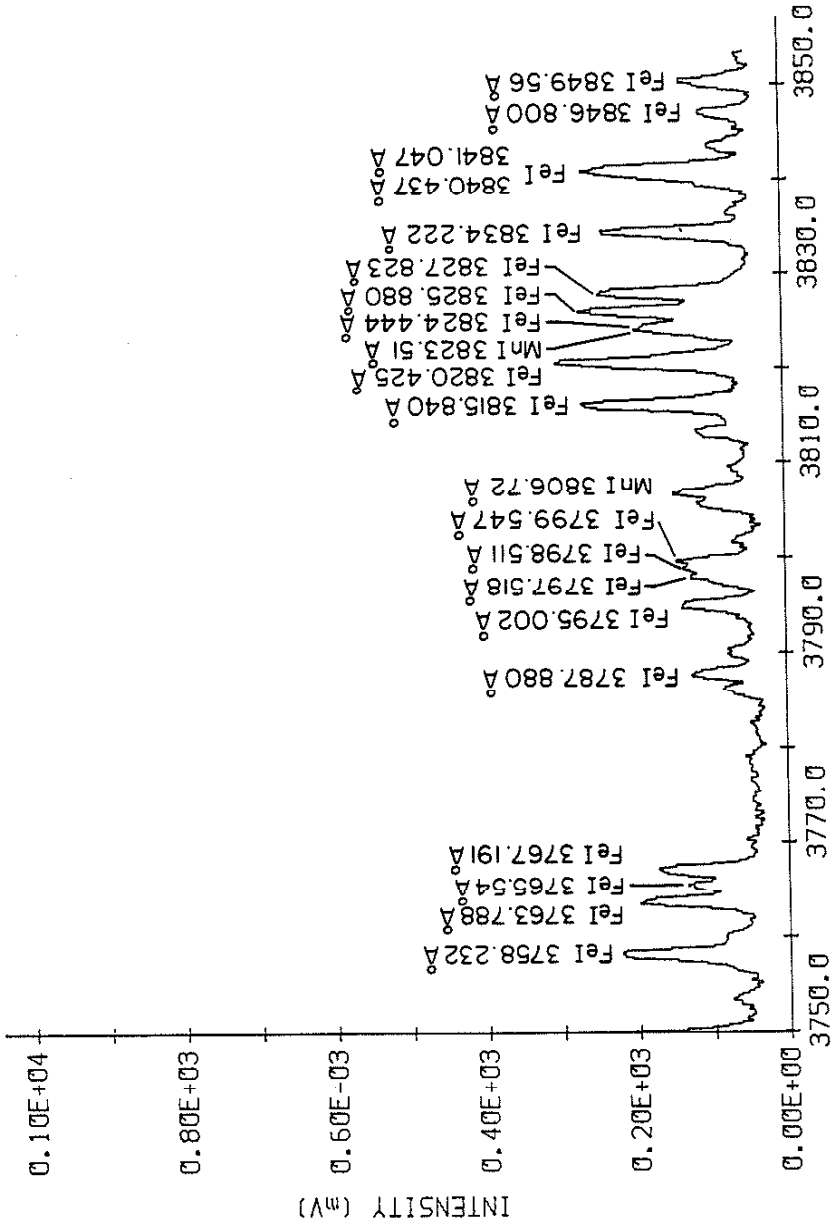

Figure A.2.7. Weld arc spectra using $Ar-O_2$ shield gas and solid wire. Wavelength region 3750 - 3850 Å.

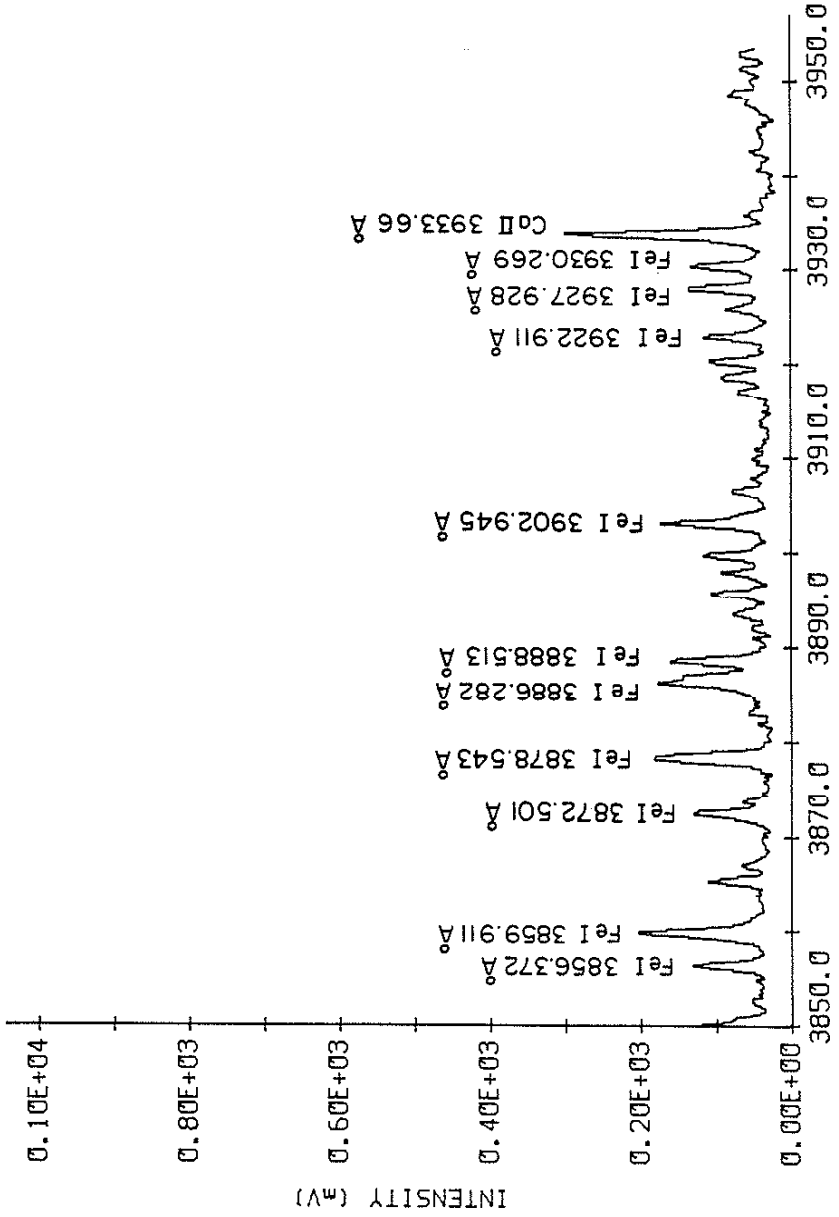

Figure A.2.8. Weld arc spectra using Ar-O_2 shield gas and solid wire. Wavelength region 3850 - 3950 Å.

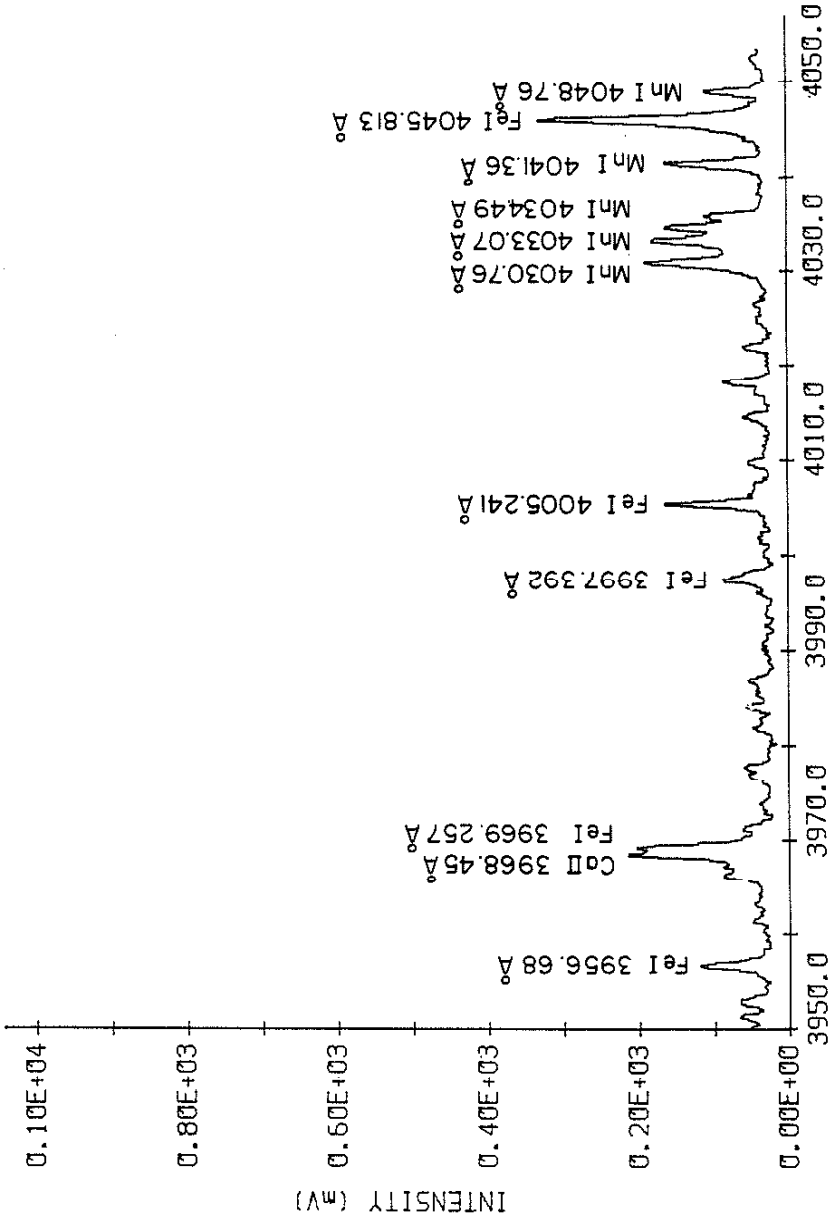

Figure A.2.9. Weld arc spectra using Ar-O_2 shield gas and solid wire. Wavelength region 3950 - 4050 Å.

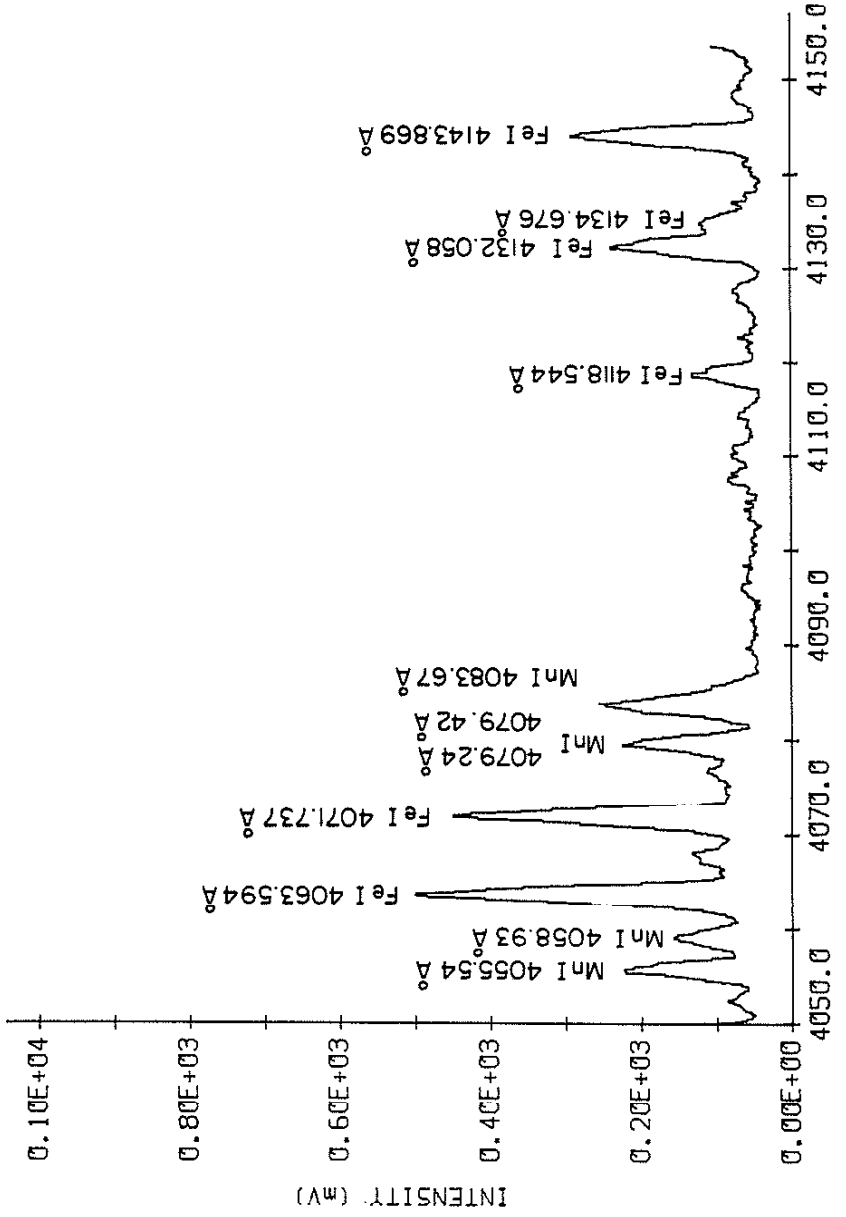

Figure A.2.10. Weld arc spectra using Ar-O_2 shield gas and solid wire. Wavelength region 4050 - 4150 Å.

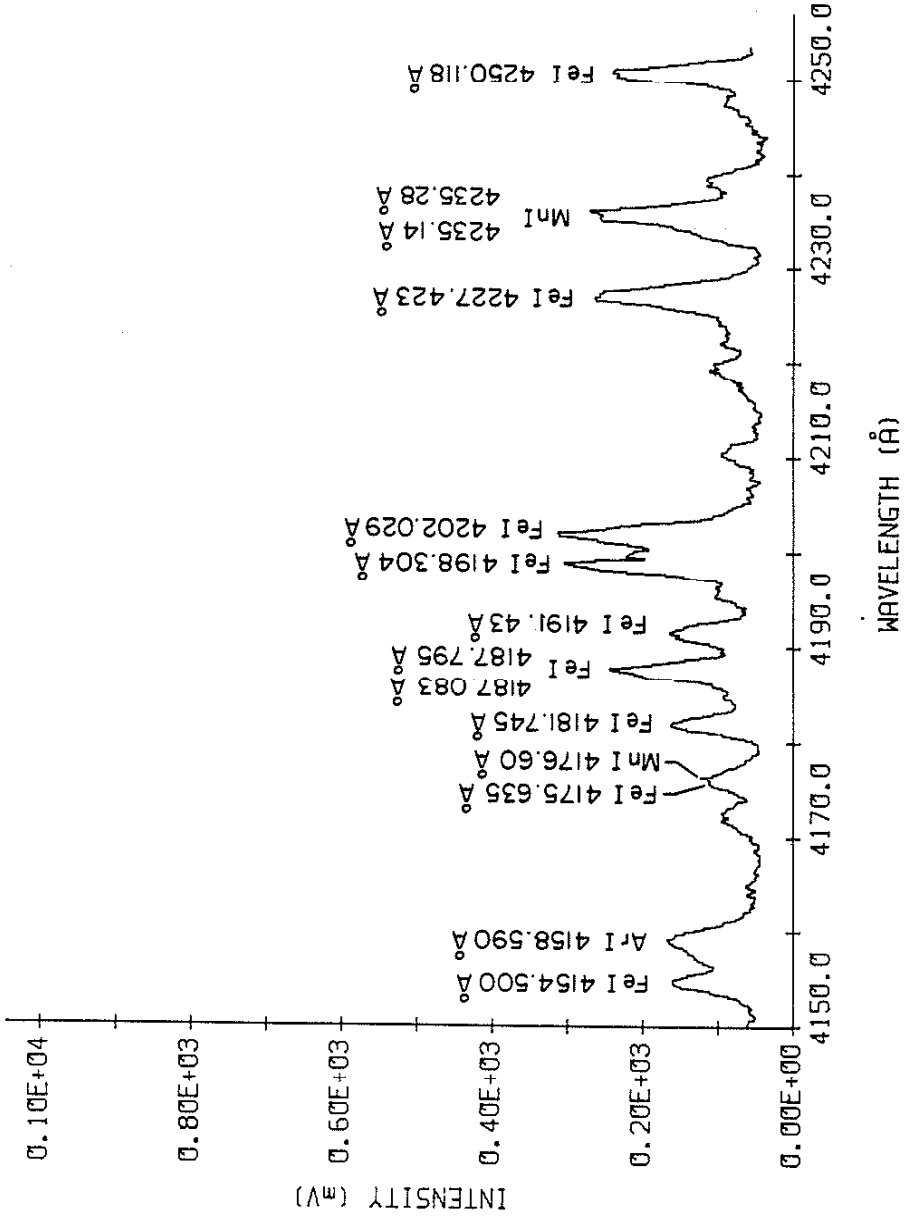

Figure A.2.11. Weld arc spectra using Ar-O_2 shield gas and solid wire. Wavelength region 4150 - 4250 Å.

A.3. Catalog of IR Spectra from 7350 - 9950 Å

Wavelengths (Å)	Filename
7350 - 7550	ALW046
7550 - 7750	ALW007
7750 - 7950	ALW007
7950 - 8150	ALW008
8150 - 8350	ALW008
8350 - 8550	ALW009
8550 - 8750	ALW009
8750 - 8950	ALW010
8950 - 9150	ALW010
9150 - 9350	ALW011
9350 - 9550	ALW011
9550 - 9750	ALW012
9750 - 9950	ALW012

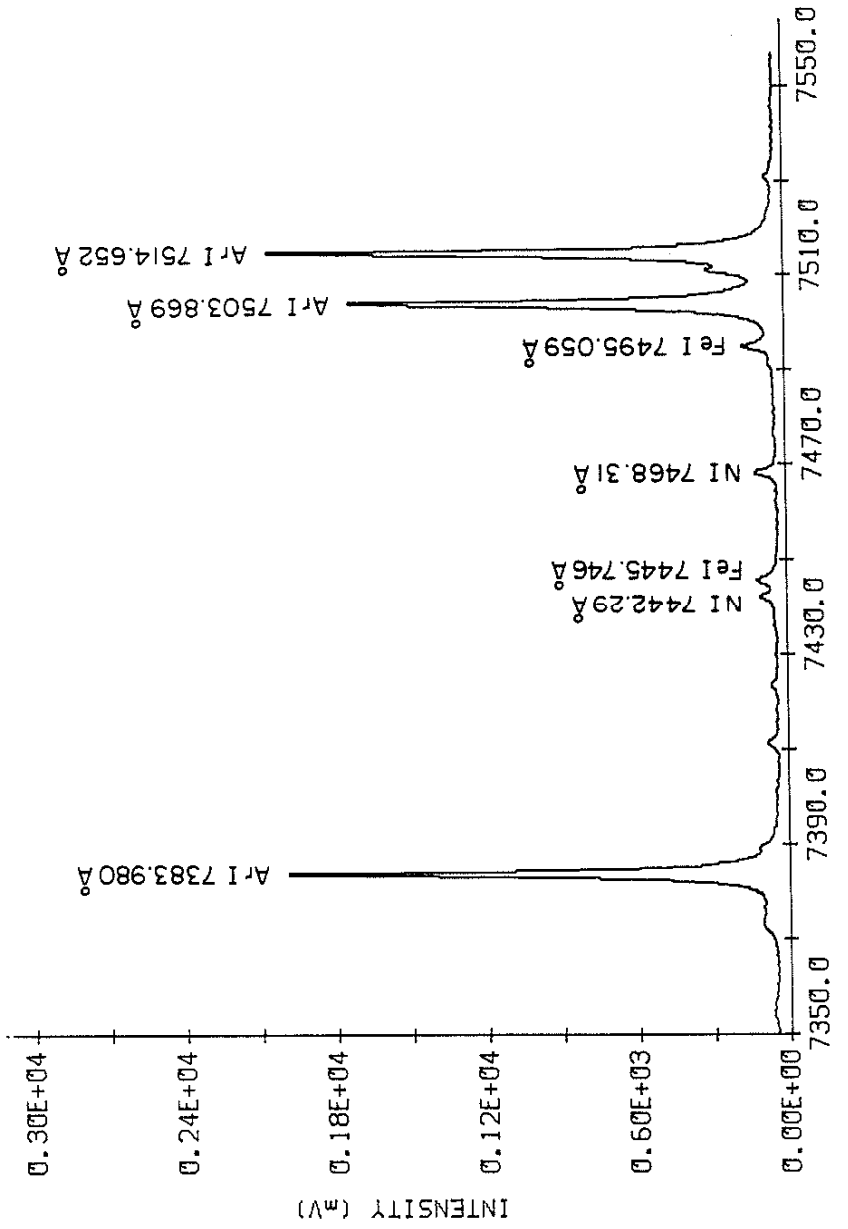

Figure A.3.1. Weld arc spectra using Ar-O_2 shield gas and solid wire. Wavelength region 7350 - 7550 Å.

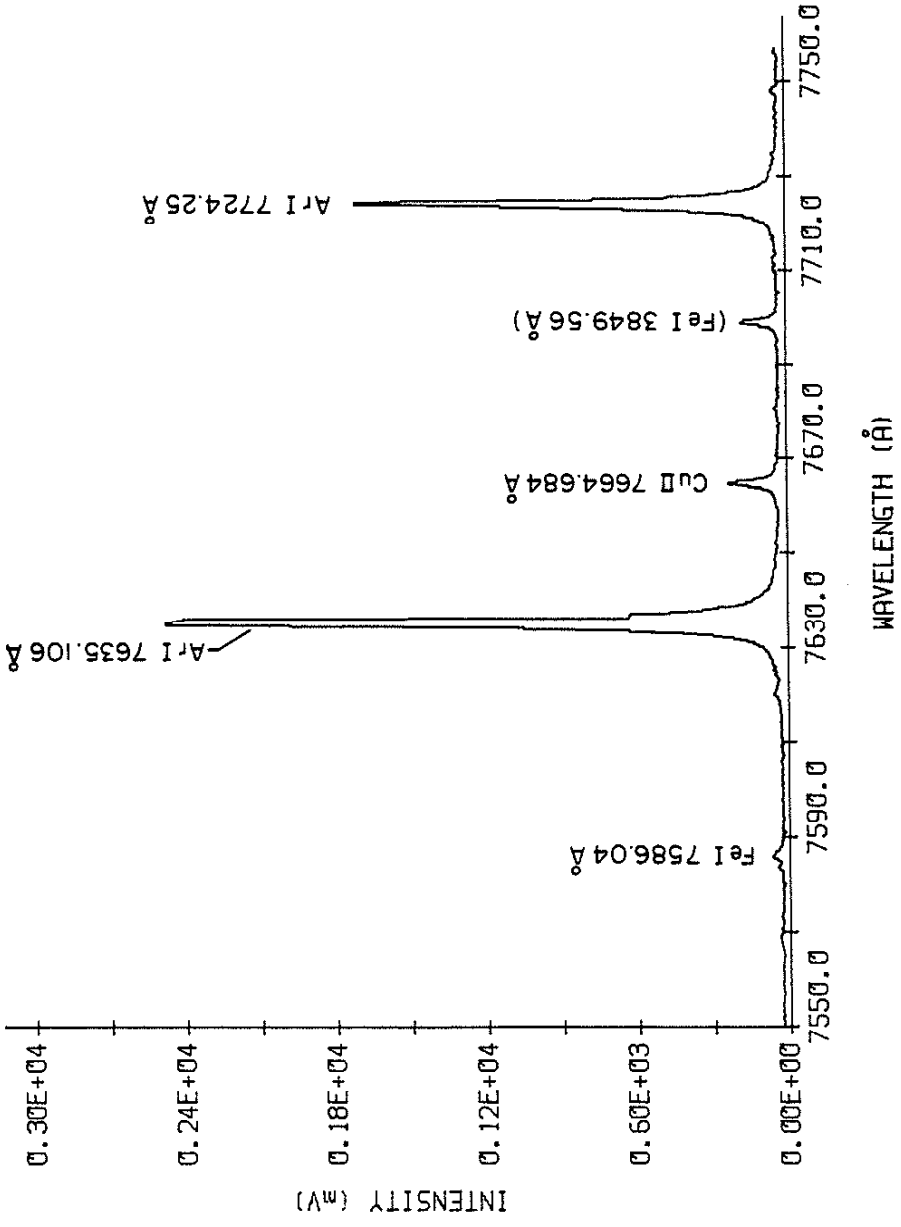

Figure A.3.2. Weld arc spectra using Ar-O_2 shield gas and solid wire. Wavelength region 7550 - 7750 Å.

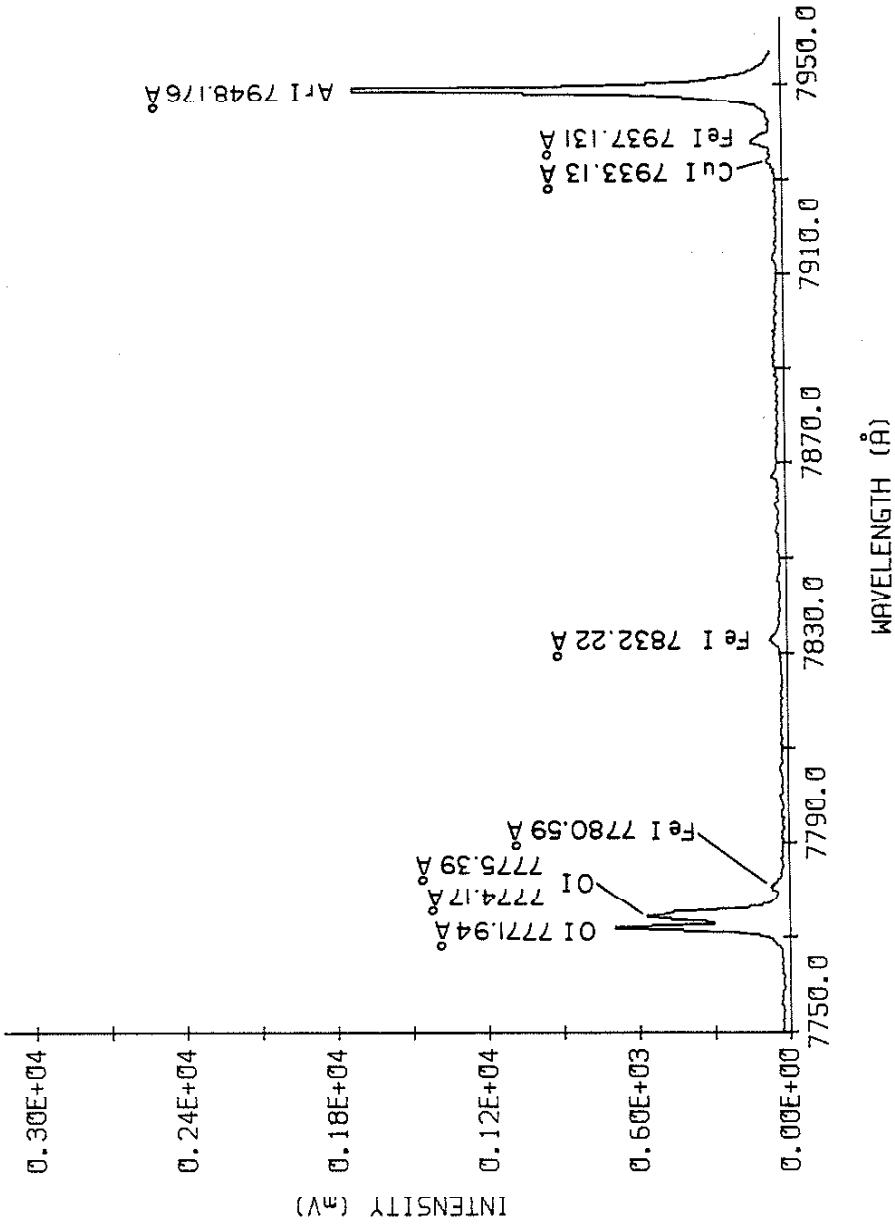

Figure A.3.3. Weld arc spectra using Ar-C_2 shield gas and solid wire. Wavelength region 7750 - 7950 Å.

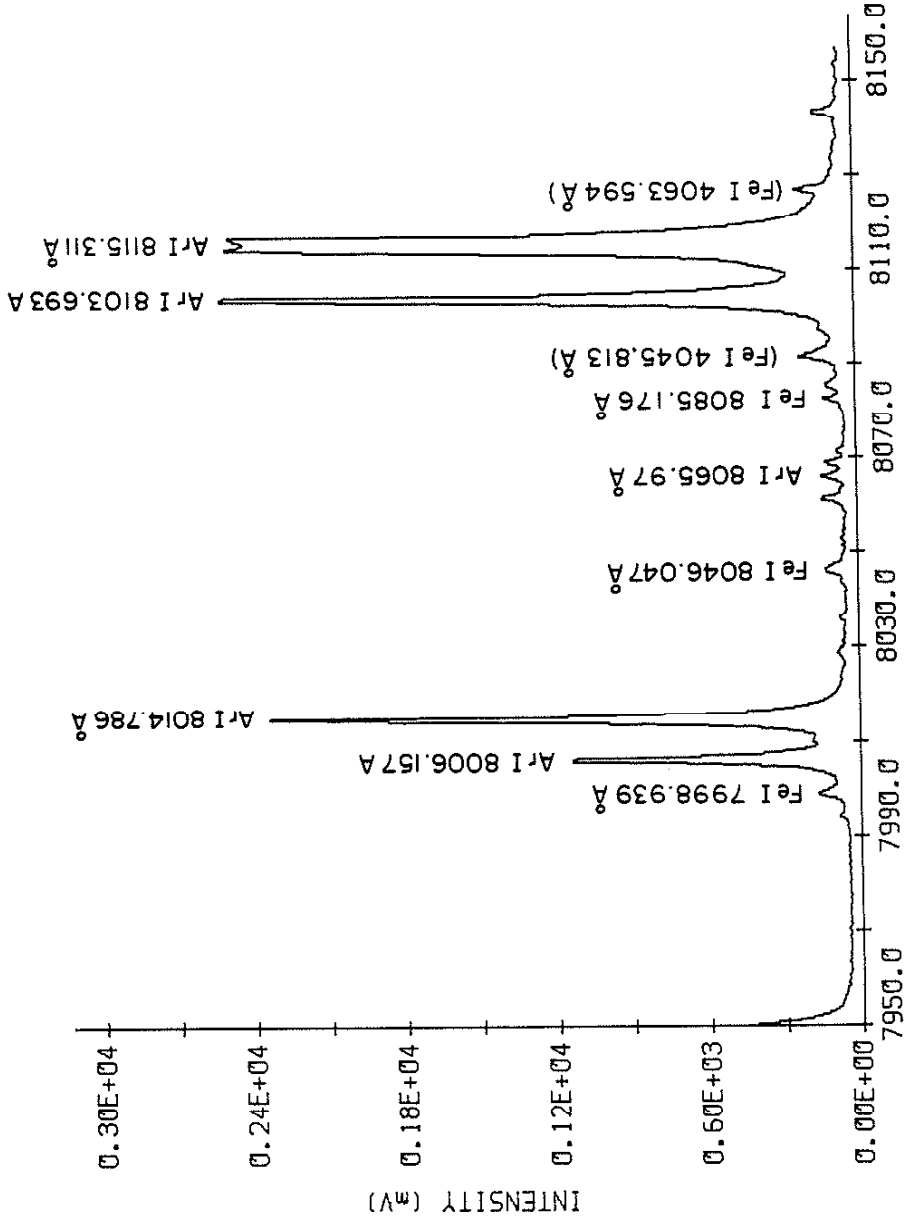

Figure A.3.4. Weld arc spectra using Ar-O_2 shield gas and solid wire. Wavelength region 7950 - 8150 Å.

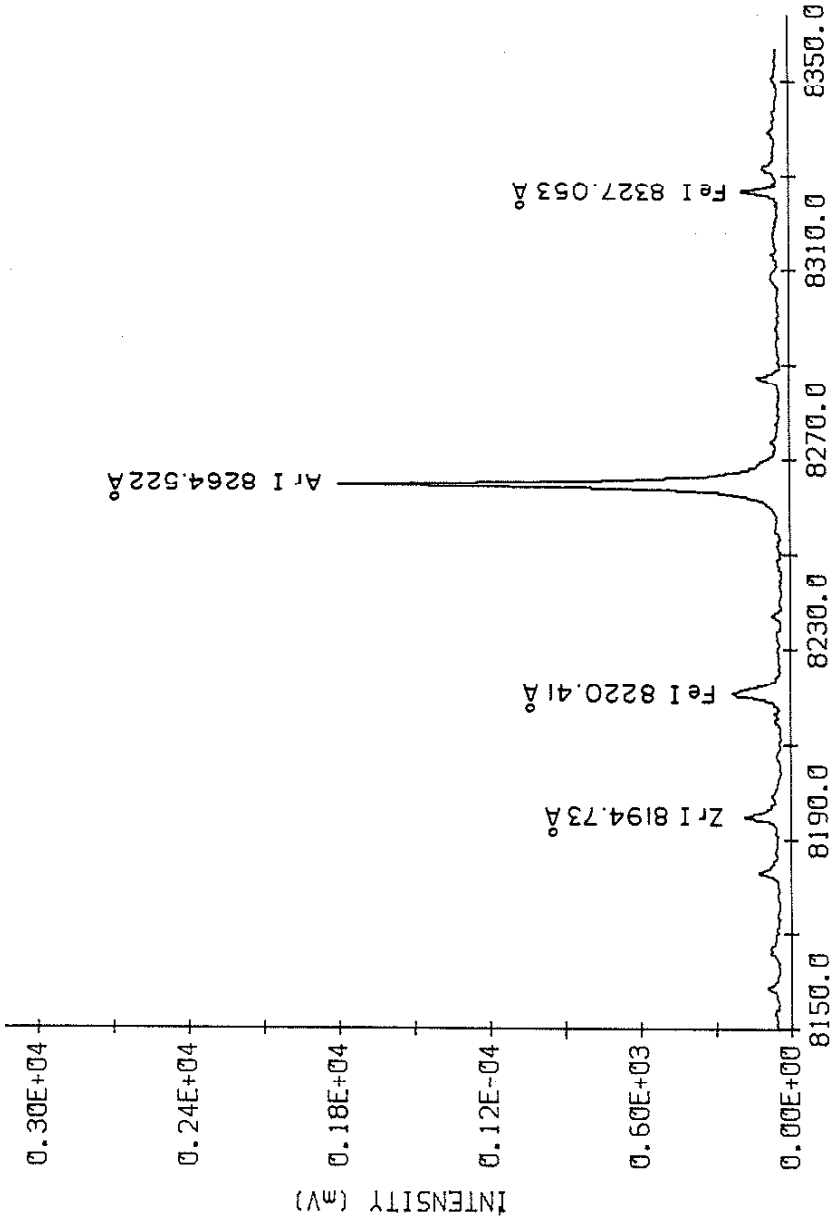

Figure A.3.5. Weld arc spectra using Ar-O_2 shield gas and solid wire. Wavelength region 8150 - 8350 Å.

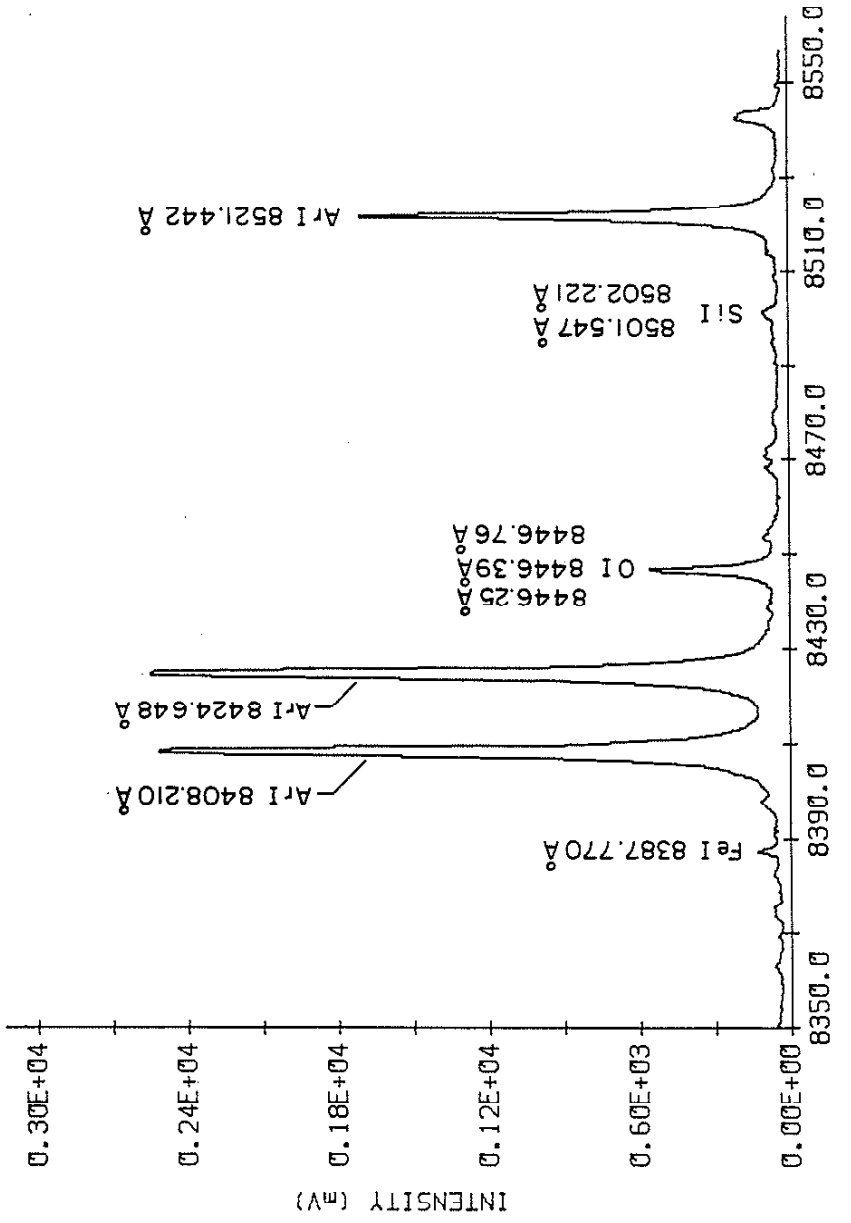

Figure A.3.6. Weld arc spectra using Ar-0_2 shield gas and solid wire. Wavelength region 8350 - 8550 Å.

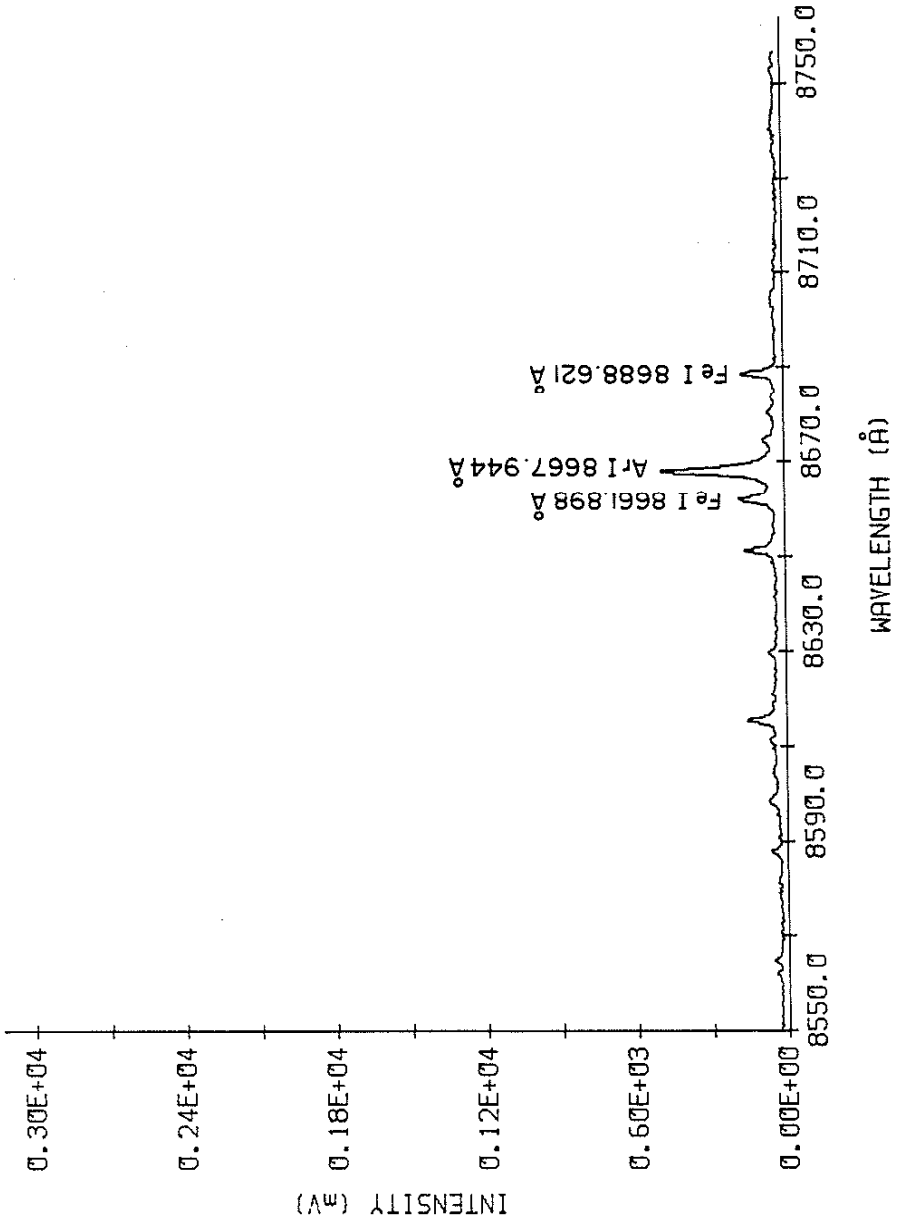

Figure A.3.7. Weld arc spectra using Ar-O_2 shield gas and solid wire. Wavelength region 8550 - 8750 Å.

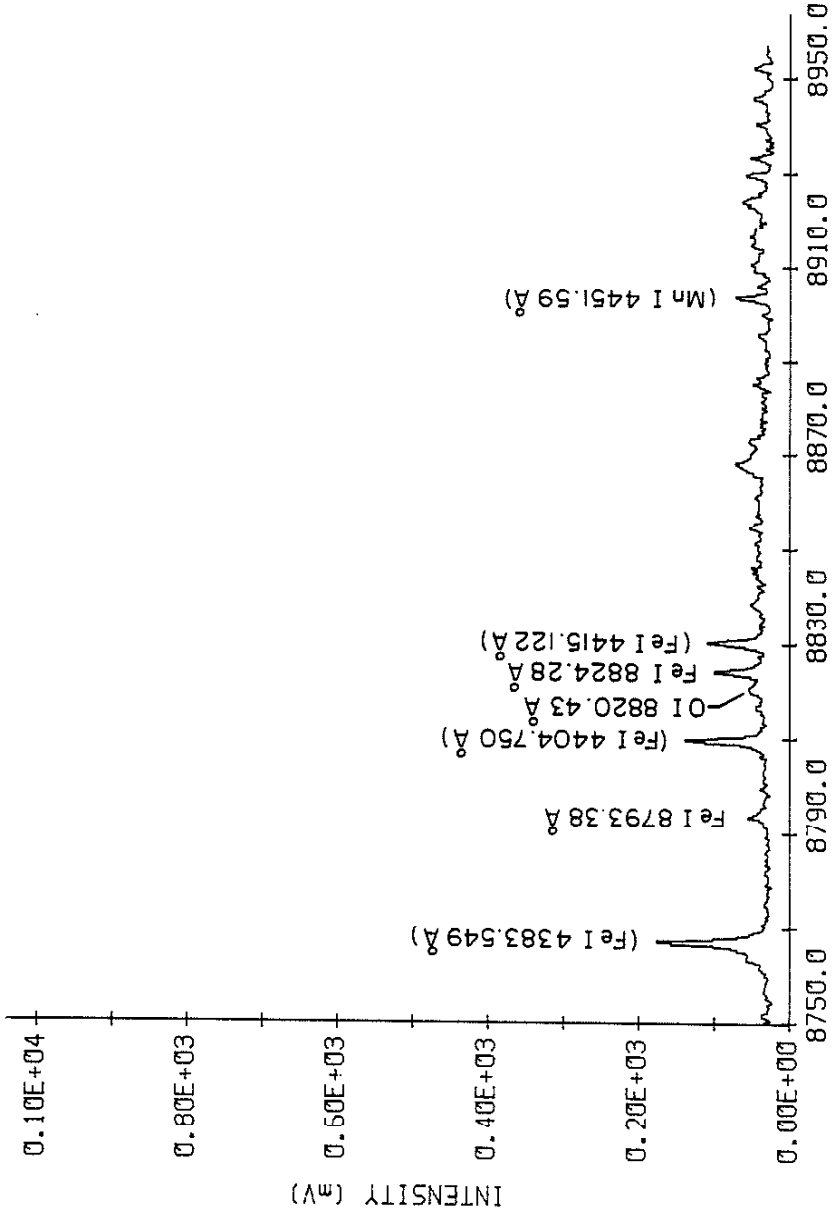

Figure A.3.8. Weld arc spectra using Ar-O_2 shield gas and solid wire. Wavelength region 8750 - 8950 Å.

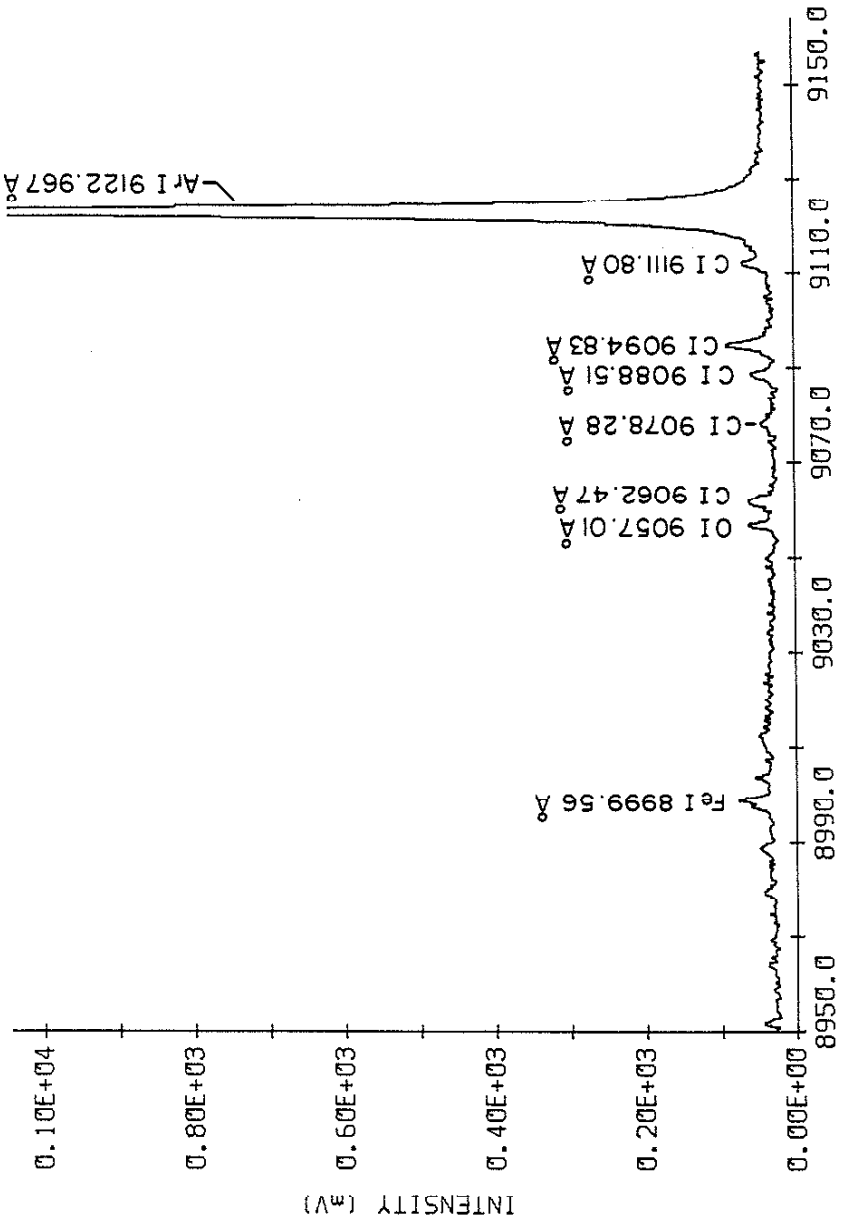

Figure A.3.9. Weld arc spectra using Ar-C_2 shield gas and solid wire. Wavelength region 8950 - 9150 Å.

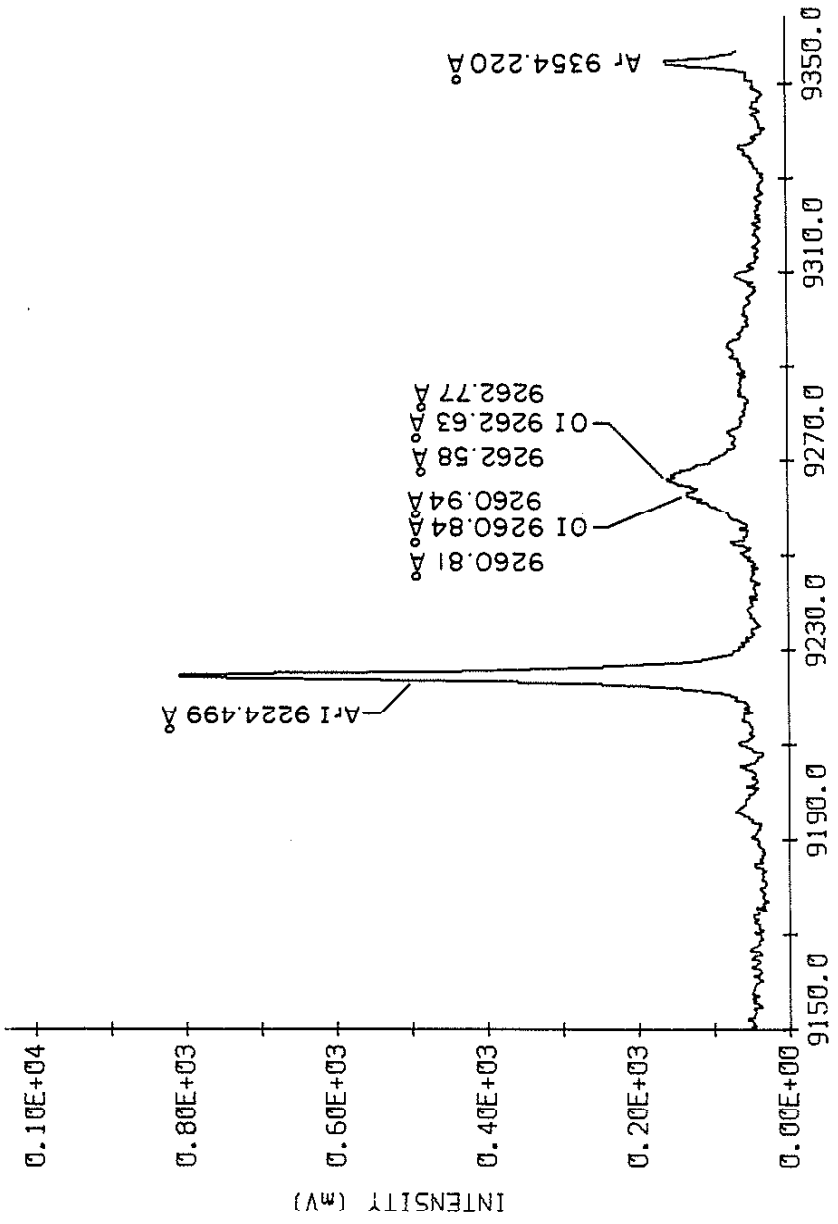

Figure A.3.10. Weld arc spectra using Ar-O_2 shield gas and solid wire. Wavelength region 9150 - 9350 Å.

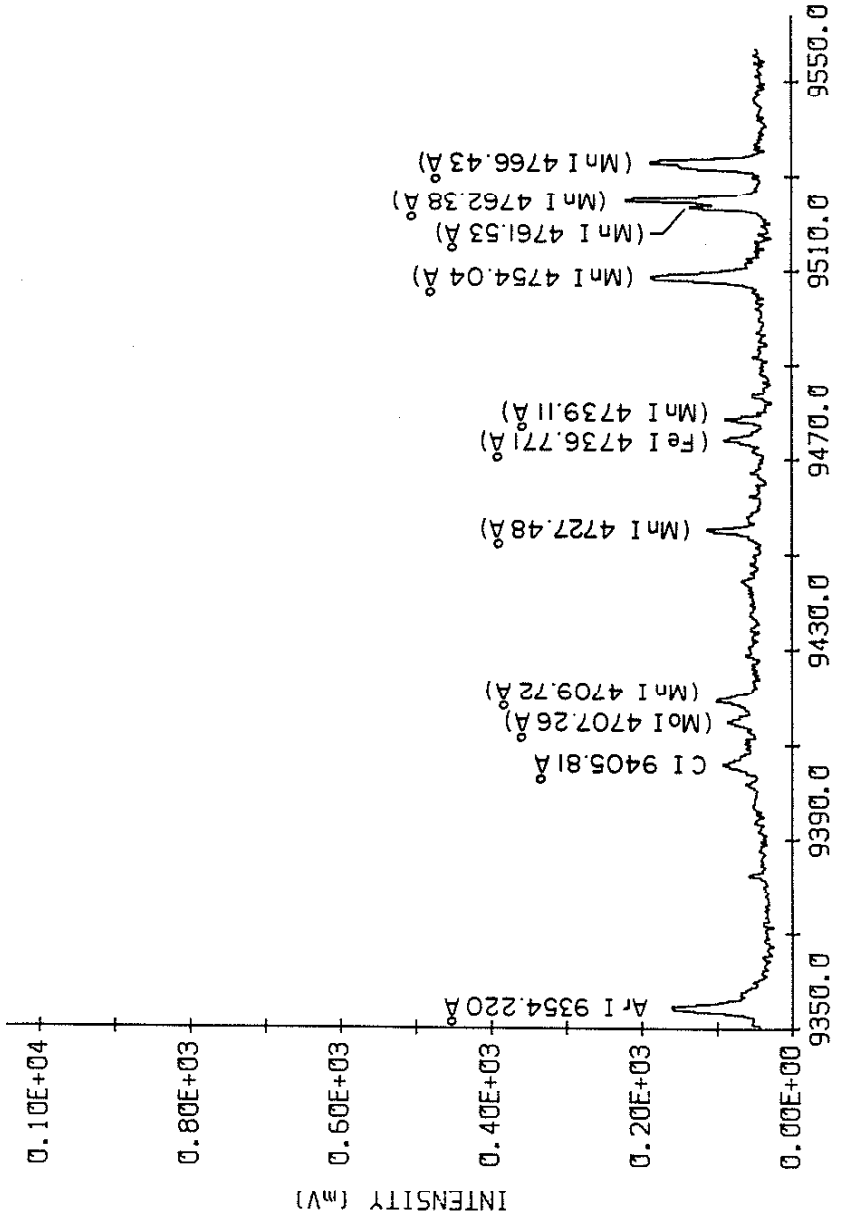

Figure A.3.11. Weld arc spectra using Ar-0_2 shield gas and solid wire. Wavelength region 9350 - 9550 Å.

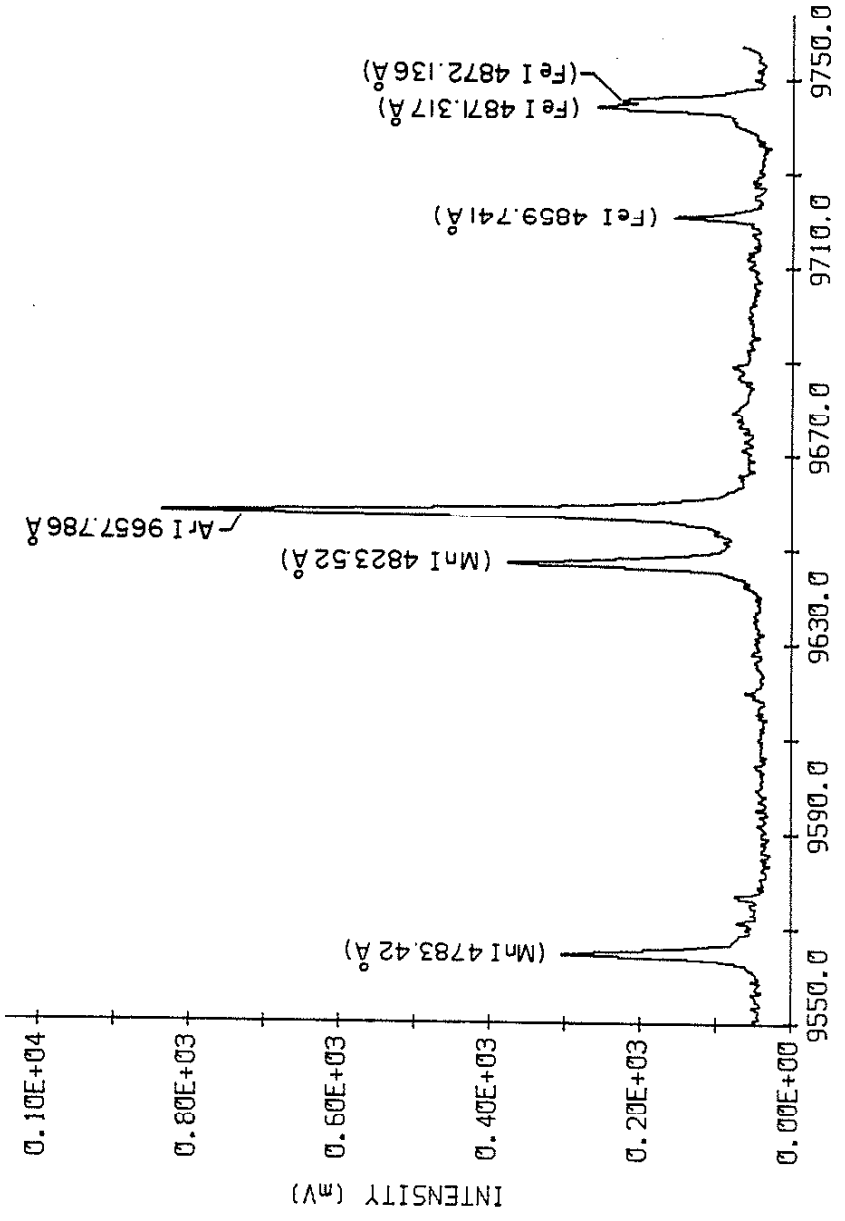

Figure A.3.12. Weld arc spectra using Ar-O_2 shield gas and solid wire. Wavelength region 9550 - 9750 Å.

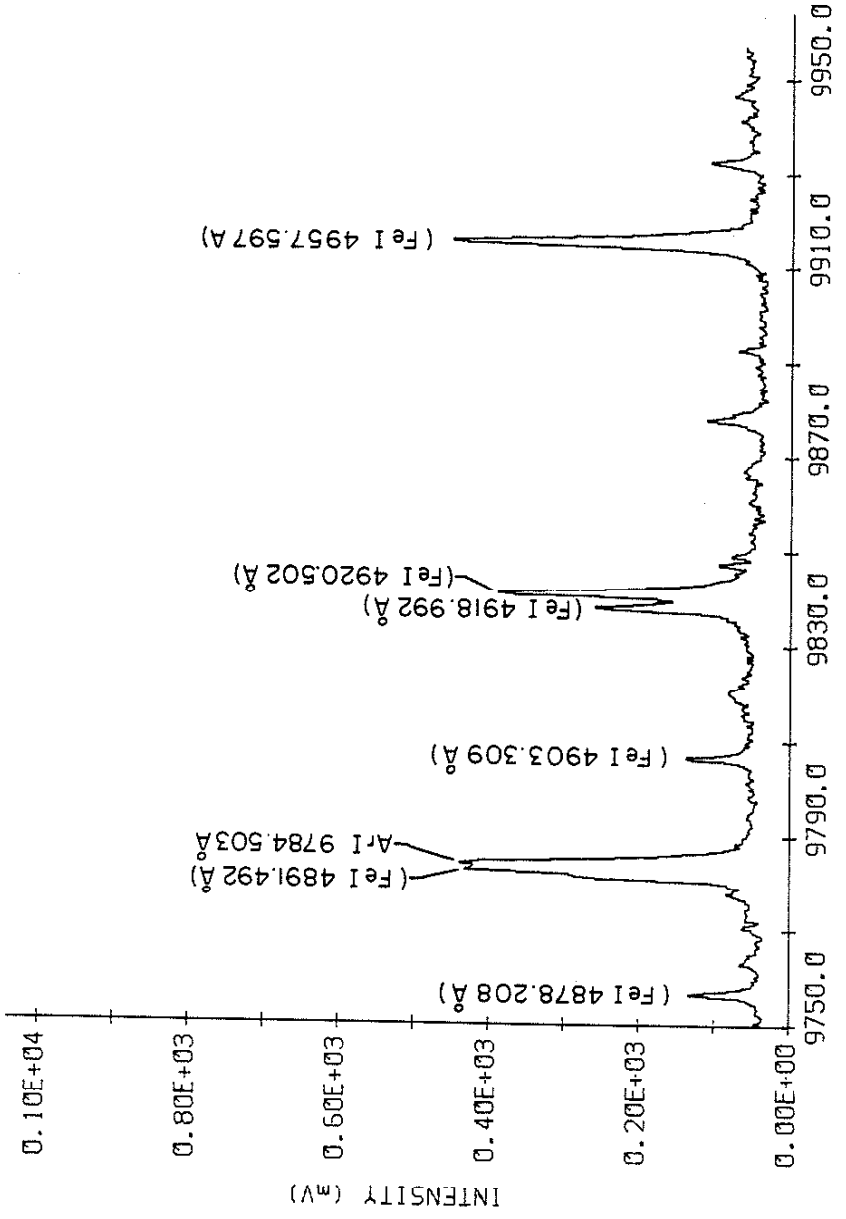

Figure A.3.13. Weld arc spectra using Ar-O_2 shield gas and solid wire. Wavelength region 9750 - 9950 Å.

APPENDIX B

FILENAMES OF SPECTRAL PLOTS FOR ABSOLUTE INTENSITY MEASUREMENTS

Ar SPECTRA

WAVELENGTHS (Å)	FILENAME	COMMENTS
	ALW118	Noise scan
6027 - 6557	ALW126	With filter
6100 - 6500	ALW121	
"	ALW121.F10	Convolved spectra with 100 Å FWHM filter
"	ALW121.F05	50 Å FWHM
"	ALW121.F02	20 Å FWHM
7600 - 8000	ALW122	
"	ALW122.UNC	Corrected for saturation
"	ALW122.F10	100 Å FWHM
"	ALW122.F05	50 Å FWHM
"	ALW122.F02	20 Å FWHM
8000 - 8400	ALW123	
"	ALW123.UNC	Corrected for saturation
"	ALW123.F10	100 Å FWHM
"	ALW123.F05	50 Å FWHM
"	ALW123.F02	20 Å FWHM

WAVELENGTHS (Å)	FILENAME	COMMENTS
8400 - 8800	ALW124	
"	ALW124.UNC	Corrected for saturation
"	ALW124.F10	100 Å FWHM
"	ALW124.F05	50 Å FWHM
"	ALW124.F02	20 Å FWHM
8800 - 9200	ALW125	
"	ALW125.F10	100 Å FWHM
"	ALW125.F05	50 Å FWHM
"	ALW125.F02	20 Å FWHM

CO_2 SPECTRA

WAVELENGTHS (Å)	FILENAME	COMMENTS
6027 - 6557	ALW134	With filter
6100 - 6500	ALW136	
"	ALW136.F10	100 Å FWHM
"	ALW136.F05	50 Å FWHM
"	ALW136.F02	20 Å FWHM
7600 - 8000	ALW137	
"	ALW137.F10	100 Å FWHM
"	ALW137.F05	50 Å FWHM
"	ALW137.F02	20 Å FWHM
8000 - 8400	ALW138	
"	ALW138.UNC	Corrected for saturation
"	ALW138.F10	100 Å FWHM
"	ALW138.F05	50 Å FWHM
"	ALW138.F02	20 Å FWHM
8400 - 8800	ALW139	
"	ALW139.F10	100 Å FWHM
"	ALW139.F05	50 Å FWHM
"	ALW139.F02	20 Å FWHM
8800 - 9200	ALW140	
"	ALW140.F10	100 Å FWHM
"	ALW140.F05	50 Å FWHM
"	ALW140.F02	20 Å FWHM

REFERENCES

[1] Kawahara, M., "Tracking Control System Using Image Sensor for Arc Welding," Automatica, vol. 19, no. 4, pp. 357-363, July 1983.

[2] de Keijzer, A. and de Groot, R. J., "Laser Based Arc Welding Sensor Monitors Weld Preperation Profile," Sensor Review, vol. 4, no. 1, pp 8-10, January 1984.

[3] Villers, P., "The Vision System Handles Parts Assembly and Weld Seam Tracking," Sensor Review, vol. 2, no. 3, pp 122-125, July 1982.

[4] Clocksin, W. F., Davey, P. G., Morgan, C. G., Vidler, A. R., "Progress in Visual Feedback for Robot Arc-Welding of Thin Sheet Steel," in Proceedings of the 2nd International Conference on Robot and Sensory Controls, Stuttgart, Germany, November 2-4, 1982, pp.189-200.

[5] Dufour, M., Cielo, P., "Optical Inspection for Adaptive Welding," Applied Optics, vol. 23, no. 8, pp. 1132-1134, April 1984.

[6] Kuhne, A.H., Frassek, B., Starke, G., "Components for Automated GMAW Process," Welding Journal, vol. 63, no. 1, pp. 31-34, Janurary 1984.

[7] "Seam Tracking - Solutions are Beginning to Emerge," Sensor Review, vol. 2, no. 2, pp. 92-94, April 1982.

[8] "Leading the Way on Robot Weld Guidance," The Industrial Robot, vol. 10, no. 2, pp. 104-107, June 1983.

[9] Wadsworth, P., "Seam Tracking Emerges in US Welding Developments," The Industrial Robot, vol. 10, no. 2, pp. 108-113, June 1983.

[10] Peterson, D., W., Ransom, P., L., "The Calibration and Cataloging of Spectral Emissions from Gas Metal Welding of Steel from 4100Å - 7450Å," RRL Report 522 (University of Illinois, Urbana, IL, 1983).

[11] Melton, G. B., "Weld Thermography," The Welding Institute, Cambridge, Project Report 3713, May 1983.

[12] Electro-Optics Handbook, Harrison, New Jersey: RCA Corp. 1974, pp. 9-21.

[13] "HR-320 Instruction Manual," Metuchen, New Jersey: Instruments S.A. Inc., 1979.

[14] Ludwig, H. C., "Plasma Energy Transfer in Gas Shielded Welding Arcs," American Welding Journal, pp. 296s-300s, 1959.

[15] Lancaster, J. F., Metallurgy of Welding, London: George Allen & Unwin Ltd., 1980, pp. 19-41.

[16] Rider, G., "Determination of Molten Weldpool using Self-Scanned Photo Diode Arrays," CEGB Report, 1978.

[17] Kobayashi, M., Suga, T., "A Method for the Spectral Temperature Measurement of a Welding Arc," Proceedings, International Conference Paper 18, 1980, pp. 25-37.

[18] Heiro H., North, T. H., "The Influence of Welding Parameters on Droplet Temperature during Pulsed Arc Welding," Welding and Metal Fabrication, vol. 44, no. 7, pp. 482-485, 1976.

[19] Rosenthal, D., "Mathematical Theory of Heat Distribution During Welding and Cutting," Welding Journal, vol. 20, no. 5, pp. 220s-234s, 1941.

[20] Rykalin, N.N., "Berechnund der Warmerorgange beim Schweissen," Verlag Tecknik, pp. 68-69, 1957.

[21] Howden, Milner, British Welding Journal, vol 10., pp. 304-316, 1963.

[22] Ramakrishnan, S., Nuon, B., "Prediction of Properties of Free Burning Welding Columns," Journal of Physics D: Applied Physics, vol. 13, pp. 1845-1853, 1980.

[23] Mills, G. S., ,"Use of Emission Spectroscopy for Arc Weld Analysis," Welding Journal, pp. 93s-96s, March 1977.

[24] Wavelengths and Transition Probabilities for Atoms and Atomic Ions, NSRDS-NBS68, Washington: U. S. Government Printing Office, 1980.

[25] Shea, J. E., Gardner C. S., "Spectroscopic Measurement of Hydrogen Contamination in Weld Arc Plasmas," Applied Physics, vol. 54, no. 9, pp. 4928-4938, September 1983.

[26] Laser Focus Buyer's Guide, Littleton, Mass.: Penwell Publishing Co., 1984.

[27] "Optics Guide 2," Irvine, California: Melles Griot Inc., 1982 pp. 242-245.

CUMULATIVE LIST OF RADIO RESEARCH LABORATORY AND
ELECTRO-OPTIC SYSTEMS LABORATORY
REPORTS PREPARED UNDER U. S. ARMY SUPPORT

RRL Rep. No. 512 - M. E. Norris and C. S. Gardner (October 1981), Microprocessor Controlled Weld Arc Spectrum Analyzer.

RRL Rep. No. 517 - Davis, R. C. and C. S. Gardner (July 1982), Spectroscopic Analysis of Laser Welding Plasma.

RRL Rep. No. 520 - Webber, D. A. and C. S. Gardner (October 1982), Evaluation of a Thermal Imaging Technique for Measuring Welding Travel Speed.

RRL Rep. No. 521 - Yang, K. S. and A. H. Schriefer, Jr. (October 1982), A Welding Table Travel Digitization System.

RRL Rep. No. 522 - Peterson, D. W. and P. L. Ransom (January 1983), The Calibration and Cataloging of Spectral Emissions from Gas Metal Arc Welding of Steel from 4100A to 7450A.

RRL Rep. No. 524 - Shea, J. E. and C. S. Gardner (February 1983), Spectroscopic Measurements of Hydrogen Contamination in Weld Arc Plasma.

RRL Rep. No. 525 - Webber, D. A. and C. S. Gardner (March 1983), An Image Correlation Technique for Measuring Weld Travel Speed.

EOSL Rep. No. 84-002 - Lenef, A. and C. S. Gardner (October 1984), Effects of Optical Emissions From Weld Arcs on the Performance of Welding Robot Vision Systems.

EOSL Rep. No. 84-003 - Houshmand, H. and C. S. Gardner (October 1984), Analysis of the Intensity Fluctuations of Optical Emission Lines in Weld Arc Plasmas.

PAPERS PUBLISHED

J. E. Shea and C. S. Gardner, "Spectroscopic measurement of hydrogen contamination in weld arc plasmas," Journal of Applied Physics, 54, 4928-4938, September 1983.